nature reviews materials

https://doi.org/10.1038/s41578-023-00582-w

Review article

Check for updates

Long-term operating stability in perovskite photovoltaics

Hongwei Zhu[1,6], Sam Teale[2,6], Muhammad Naufal Lintangpradipto[1], Suhas Mahesh[2], Bin Chen[2], Michael D. McGehee[3], Edward H. Sargent[2,4,5] ✉ & Osman M. Bakr[1] ✉

Abstract

Perovskite solar cells have demonstrated the efficiencies needed for technoeconomic competitiveness. With respect to the demanding stability requirements of photovoltaics, many techniques have been used to increase the stability of perovskite solar cells, and tremendous improvements have been made over the course of a decade of research. Nevertheless, the still-limited stability of perovskite solar cells remains to be fully understood and addressed. In this Review, we summarize progress in single-junction, lead-based perovskite photovoltaic stability and discuss the origins of chemical lability and how this affects stability under a range of relevant stressors. We highlight categories of prominent stability-enhancing strategies, including compositional tuning, barrier layers and the fabrication of stable transport layers. In the conclusion of this Review, we discuss the challenges that remain, and we offer a perspective on how the field can continue to advance to 25-year and 30-year stable perovskite solar modules.

Sections

[1]KAUST Catalysis Center, Division of Physical Sciences and Engineering, King Abdullah University of Science and Technology, Thuwal, Kingdom of Saudi Arabia. [2]Department of Electrical and Computer Engineering, University of Toronto, Toronto, Ontario, Canada. [3]Materials Science and Engineering Program, University of Colorado Boulder, Boulder, CO, USA. [4]Department of Chemistry, Northwestern University, Evanston, IL, USA. [5]Department of Electrical and Computer Engineering, Northwestern University, Evanston, IL, USA. [6]These authors contributed equally: Hongwei Zhu, Sam Teale. ✉e-mail: ted.sargent@northwestern.edu; osman.bakr@kaust.edu.sa

Introduction

Because of their remarkable properties, metal-halide perovskite (MHP) semiconductors have ushered in a new era of solar cell research. MHPs form an ABX_3 structure in which the A site is a monovalent cation (typically a mixture of caesium, methylammonium or formamidinium), the B site is a divalent metal (usually Pb or Sn) and the X site is a pure halide or mixture of halides (I, Br, Cl) (Fig. 1a). Owing to their large absorption coefficients, high mobilities, long diffusion lengths and tunability, polycrystalline thin films of perovskite have been used to fabricate perovskite solar cells (PSCs) with bandgaps from 1.2 to 2.3 eV (refs. 1,2) and power conversion efficiencies (PCEs) approaching 26% (~1.5 eV)[3]. Metal-halide perovskites are commonly known to have intrinsic defect tolerance, but modest temperatures (≥60 °C) can cause perovskite crystal decomposition[4,5], and 1-sun illumination can break bonds to induce degradation[6,7]. Unsurprisingly, the time taken for early PSCs to drop to 80% of their original performance (their T_{80} lifetime) was only a few hours[8]. Since then, great strides have been made, and some PSCs have demonstrated thousands of hours of operational stability at ≥65 °C with negligible PCE loss[9,10]. Despite these improvements, the fundamental understanding of instabilities and the mechanisms behind stability-enhancing methods are often overlooked.

In this Review, we focus on lead-based perovskites used in single-junction PSCs. First, we discuss the special properties of perovskite materials and the major advances in PSC stability. Then we discuss the factors affecting PSC stability, the techniques used thus far to combat them, and potential routes to further improvement. Several reports have demonstrated encapsulation that renders humidity and oxygen effects negligible on timescales up to 1 year (ref. 11). Hence, it seems reasonable to consider moisture and oxygen ingress separately as an encapsulation issue. The need for robust, long-term encapsulation techniques and the best ways to encapsulate PSCs are discussed at length elsewhere[12]. Here, we instead focus on illumination, bias and temperature-based degradation.

Differences between perovskites and traditional semiconductors

Perovskites and traditional semiconductors (such as Si, CdTe and III–V semiconductors) have several key differences (Fig. 1a,b) that ultimately affect their stability. Paramount to the success of perovskites is their defect tolerance, a result of their band structure (Fig. 1a, right). In typical semiconductors, the valence band maximum (VBM) is formed from bonding orbitals and the conduction band minimum (CBM) from antibonding orbitals[13]. When these bonds are broken, dangling bonds form close to where the original bonds were, creating defects deep within the semiconductor bandgap (Fig. 1b, right). Perovskites instead form their bandgap from antibonding orbitals at both the VBM and CBM, and thus breaking these bonds produces states away from the bandgap, either shallow defects or states within the valence band. The upshot of this is that polycrystalline perovskite films with defect densities 10^6 times greater than single-crystal silicon can produce similar solar cell performance[14]. The downside is that high defect densities reduce the energy needed for ions to migrate through the film, and defects tend to propagate over time, resulting in faster degradation of the absorber[15].

A second important difference between perovskites and traditional semiconductors is the lone pair effect. The divalent metal B site (usually Pb or Sn) forms with a lone pair of electrons that dictates the local geometry of the perovskite lattice[16] (Fig. 1c). Similarly to how a water molecule is bent by the lone electron pairs on the oxygen, the perovskite lattice is distorted by the lone pair on the B site. However, rather than distorting to one specific orientation (like in the case of water), several local minima exist, and at room temperature the perovskite lattice is continually moving and reorienting. This behaviour is not clearly resolved by X-ray diffraction, which reveals the average lattice spacing, but is obvious in the Raman spectra of perovskites, which at room temperature appear similar to fluids[17] (Fig. 1d). The dynamic nature of the perovskite lattice has many profound consequences for its stability. The thermal expansion coefficients of metal-halide perovskites are typically 10 times that of silicon, which is an important consideration when evaluating the mismatch in expansion and thus strain between perovskite and contacts. Additionally, the dynamic lattice increases the density of interstitials and vacancies, and aids ion migration[16].

Ion migration is of great consequence in perovskite photovoltaics. High defect densities generate high ion densities (up to 10^{17} cm^{-3}) (ref. 18) and provide pathways for ion migration through the lattice or along grain boundaries. The ion migration energy of halides is lower than for cations or metal species[19], meaning halide drift is generally attributed as the reason that perovskites act as both electronic and ionic conductors. PSCs are typically made by sandwiching a mostly intrinsic perovskite semiconductor layer between an electron-transport layer (ETL) and a hole-transport layer (HTL). Mobile ions in the perovskite migrate to the interfaces until they screen the built-in electric field that would normally exist when a semiconductor with a relatively low carrier density is between electrodes with different work functions. If the voltage across a PSC is changed so quickly that the ions cannot redistribute fast enough, then, depending on the direction of the voltage scan, the field can either be larger than normal (which favours electron extraction) or it can point in the wrong direction (which hinders electron extraction)[18]. On initial testing, hysteresis is measured between forward and reverse current–voltage (J–V) scans with strong dependency on scan speed[20,21]. In the long term, ion redistribution results in a loss of current over time due to either flattening bands at the device interface or a build-up of insulating interface material[22]. More troublingly, we now know that in iodide-based MHPs, the density of mobile ions is increased under illumination. As the VBM is formed from iodide bonds, photogenerated holes could oxidize iodide to make neutral iodine interstitials and iodide vacancies (Fig. 1e) causing several knock-on effects: iodine interstitials act as recombination centres and, because iodide vacancies are conductive, they move towards the interfaces[23,24], I_2 gas is produced and can leave the perovskite, and iodine ions diffuse into charge-transport layers (CTLs) where they can react with metal electrodes, reducing conductivity[25] (Fig. 1f).

Another phenomenon that affects perovskite stability is phase segregation under illumination. For most perovskites in the family $AB[I_{1-x}Br_x]_3$, iodine and bromine can be mixed uniformly for x ranging from 0 to 1. However, typically when x is greater than 20–33%, the perovskite phase separates into iodide-rich and bromide-rich regions under illumination[26]. The characteristic demonstration of this phase segregation is redshifted photoluminescence. When the film absorbs light, electrons and holes migrate to (lower-energy) iodide-rich regions, and as segregation progresses, the photoluminescence redshifts over time (Fig. 1g). The fundamental driver for segregation is debated, some suggesting it is thermodynamic in origin[27,28], others suggesting it is the result of polaron-induced lattice strain[29,30] or charge carrier gradients[31,32]. Some consensus is emerging that iodide is oxidized by photogenerated holes and has a higher mobility than bromine, and this sets up the opportunity for halide segregation[33,34]. Regardless, phase segregation limits the potential open-circuit voltage (V_{OC}) of ≥1.7-eV-bandgap PSCs necessary for tandem photovoltaics.

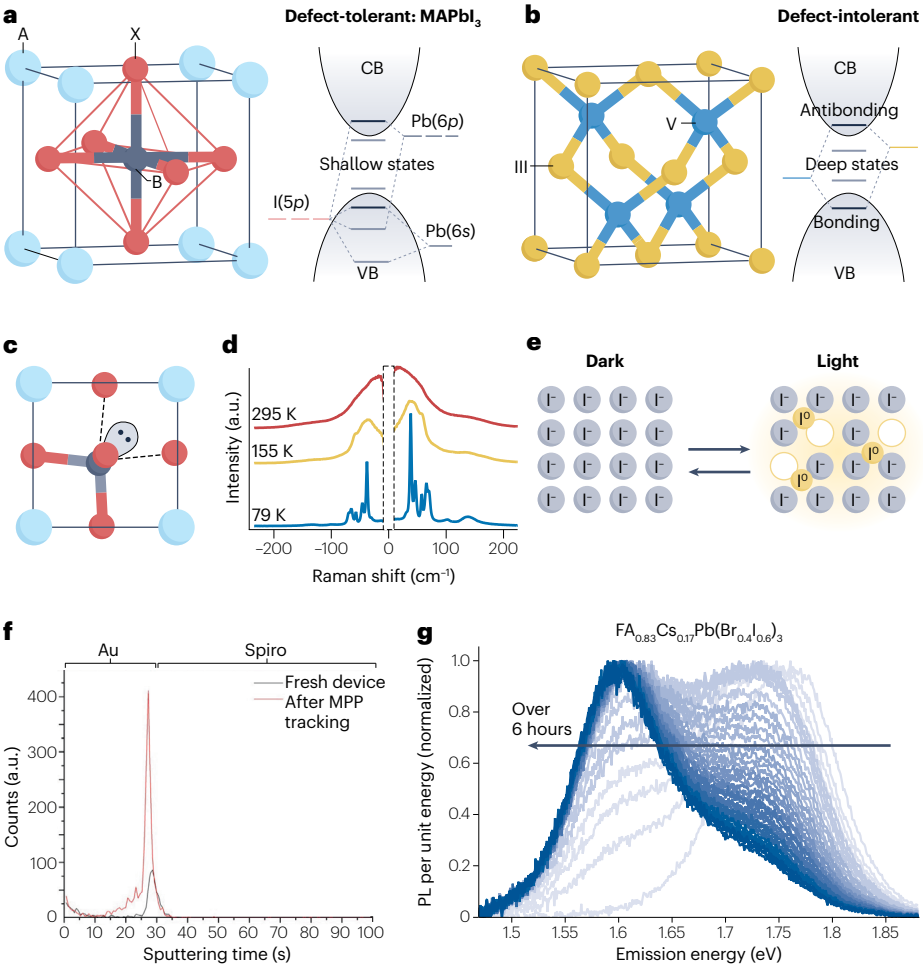

Fig. 1 | The unusual properties of perovskite semiconductors. a, The crystal structure of perovskite semiconductors (left) and the accompanying band structure (right). **b**, The crystal structure of traditional III–V semiconductors (left) and the accompanying band structure (right). **c**, Illustration of lattice distortion due to the lone pair effect in perovskite semiconductors. **d**, Temperature-dependent Raman spectra of $MAPbBr_3$ demonstrating the fluid-like bonding nature of metal-halide perovskites at room temperature. **e**, Schematic of light-induced ionic restructuring in iodine-based perovskites. **f**, Time-of-flight secondary ion mass spectroscopy showing a build-up of iodine ions at the metal/hole-transport layer interface after ageing a perovskite solar cell. The build-up is due to halide diffusion through charge-transport layers. **g**, Photoluminescence (PL) measurements of a 40% Br film, showing the increase of emission from iodine-rich regions as a function of illumination time. CB, conduction band; MPP, maximum power point; VB, valence band. Panel **a**, right, adapted from ref. 13, CC BY 4.0. Panel **b**, right, adapted from ref. 13, CC BY 4.0. Panel **c** adapted from ref. 16, Springer Nature Limited. Panel **d** adapted with permission from ref. 17, APS. Panel **e** adapted with permission from ref. 195, Max Planck Institute for Solid State Research. Panel **f** reprinted with permission from ref. 196. Copyright 2019 American Chemical Society. Panel **g** reprinted from ref. 197, CC BY 4.0.

Device stability so far

The PCE of PSCs now rivals that of Si photovoltaics (PV), and thus device stability is of utmost importance. The stability of PSCs depends on many factors (ageing condition, perovskite composition, CTLs, electrodes, encapsulation and passivation) and is thus a complex issue. Considering ageing conditions alone, a consensus statement on stability testing of PSCs was made in 2020 (ref. 35), and researchers are encouraged to use the ISOS testing protocols to enable comparison between studies. PSCs are classified into two architectural configurations: conventional (n–i–p) and inverted (p–i–n) structures (Fig. 2a,b). Figure 2c shows a timeline of PSCs, comparing record certified efficiency in n–i–p and p–i–n cells along with reported stability. We find that even though the efficiency of the record n–i–p devices has improved hugely in the past decade, their stability has improved relatively slowly (Box 1). Some reports on record devices are without stability measurements, others use different device fabrication with lower efficiency for stability testing and those that use the same architecture record T_{80} lifetimes at room temperature of only a few hundred hours[36]. These results give the impression that poor stability is abundant among the best PSCs. Scrutinizing further, one finds that the situation is more positive. The stability of record p–i–n devices, for example, has vastly improved, with devices demonstrating stability under illumination and heat (ISOS-L2/3) with T_{80} > 1,000 h from initial PCEs >23%. It should be noted that similarly high stability has been demonstrated in n–i–p, but not with record efficiency[8,10,22]. Indeed, we also notice that many impressive stability milestones have been achieved. These are generally accomplished with low-efficiency devices first, and a few years is taken to achieve the same stability in a device with record efficiency.

Factors other than ageing condition that affect perovskite stability are often considered separately from efficiency, with many reports using CTLs or metal contacts for their stability testing that are different from those used to obtain their best PCEs. This is particularly popular in n–i–p devices where the hole-transporting material (HTM) spiro-OMeTAD is replaced with more stable HTMs[37–40]. This causes two problems: stability is achieved with significantly lower (often unreported) PCEs than the best efficiencies, and cells are optimized for efficiency using spiro-OMeTAD when these optimizations may not be beneficial using other CTLs. As the field matures, it is important to combine stability with efficiency, considering how best to optimize devices within a stable architecture.

Another development is outdoor perovskite stability testing. Initially, real-world testing produced T_{80} lifetimes of only a few days[41]. More recently, however, the use of lamination-based glass–glass encapsulation has produced cells with no PCE degradation after

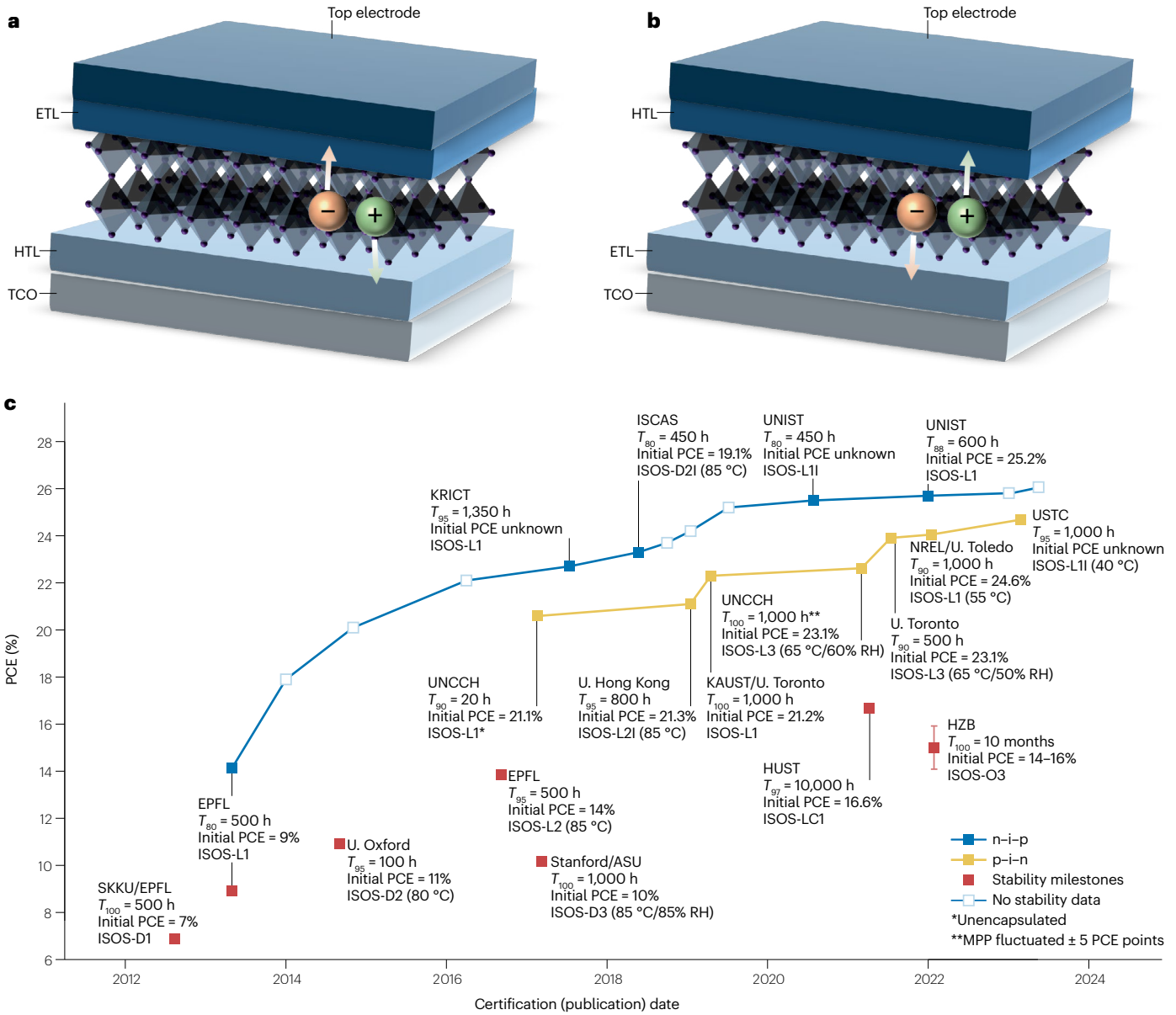

Fig. 2 | Timeline for stability in perovskite solar cells. a,**b**, The configuration of typical p–i–n (**a**) and n–i–p (**b**) perovskite solar cells (PSCs). **c**, A timeline for stability among PSCs with record efficiency. The blue and yellow lines represent record certified efficiency (steady-state) in n–i–p and p–i–n, respectively, whereas the red squares denote the earliest report of certain stability milestones: D1, dark storage (room temperature); D2, dark storage (high temperature); D2I, L1I and L2I, corresponding tests carried out in an inert atmosphere (intrinsic stability testing); D3, dark storage (high temperature + high humidity); L2, maximum power point (MPP) tracked under illumination (high temperature); LC1, light-cycled (room temperature); O3, outdoor testing at MPP. ETL, electron-transport layer; HTL, hole-transport layer; PCE, power conversion efficiency; RH, relative humidity; TCO, transparent conductive oxide. References can be found in Supplementary Table 1.

10 months of maximum-power- point (MPP) tracking outdoors in Berlin[42] (Fig. 2c). A small-scale (~3-m^2 active area) perovskite solar farm with lamination encapsulation and an initial efficiency ~12.5% PCE was tested over the course of a year, with a recorded T_{80} of 5,832 h (8 months) following the ISOS-O3 protocol[43]. These results indicate that the lifetime of PSCs is increasing beyond what is practically assessable, and there is a need to move from standard test conditions towards accelerated testing.

Factors affecting PSC stability

To understand the rapid increase in PSC stability and how to improve it further, we must first understand which materials and stressors contribute. Despite differences in configuration between n–i–p and p–i–n devices, both consist of similar layers: the electron-transporting layer (ETL), hole-transporting layer (HTL), perovskite light-absorbing layer, cathode and anode contacts (Fig. 2a,b). Under different external stressors (that is, illumination, thermal and bias), the instability

of each constituent layer and the interfaces between layers are both important factors leading to operational instability.

Perovskite stability

Inherent stability of perovskite structure/phase. Before delving into the stability of full PSCs, we should examine the intrinsic stability of the perovskite structure. The majority of highly efficient PSCs are based on a 3D perovskite in a cubic crystal phase (also known as the α-phase). The Goldschmidt tolerance factor τ can be used to determine the stability of a given perovskite from the ionic radii of its constituent ions:

$$\tau = (R_A + R_X)/\sqrt{2}(R_B + R_X),$$

where R_A, R_B and R_X are the ionic radii of the corresponding ions. In general, if τ for a given perovskite composition is between 0.9 and 1.0, it forms an ideal cubic structure. If τ is between 0.71 and 0.9, it will form an orthorhombic structure around room temperature. For MHPs, as an advantage of the configuration[141,158,199]. Still, this equivalence is bolstered when considering our 26 recent data points with high stability, which are evenly spread between n–i–p and p–i–n (Supplementary Fig. 1). Finally, we find that the vast majority of PSC stability is reported in cells with bandgaps from ~1.5 eV to 1.65 eV (panel **d** of the figure). This result is unsurprising as most PSC research is in this range, but demonstrates the need for more work in the areas of low-bandgap (~1.2 eV Pb/Sn) and wide-bandgap (~1.8 eV) cells that are used in all-perovskite tandems. Although not the subject of this Review, it should be noted that in Pb-free, Sn-containing perovskites, the oxidation of Sn(II) to Sn(IV) results in poorer stability for narrow-bandgap PSCs[200]. Additionally, higher ionic conductivity and halide segregation hamper the stability of wide-bandgap films with >20% Br concentration[201].

Box 1

The Perovskite Database

An open-access database of perovskite solar cell (PSC) results has been generated with data from >40,000 devices published between 2012 and 2020 (ref. 198), most of which have no stability data associated with them. Still, there are >1,000 devices with stability referenced to the ISOS protocols, which we used to generate the figure.

Panel **a** of the figure compares stability over time from all PSCs in the Perovskite Database with corresponding ISOS protocols. The data are understandably noisy, as there are various perovskite compositions, device architectures and ageing parameters included. The trendline still demonstrates an increase in T_{80} lifetime from ~10 h to ~100 h over 6 years. However, noise brought about by the huge volume of studies under-represents the stability gains. Looking instead at only PSCs aged under illumination (see the figure, panel **b**), the increase in stability from 2015 to 2020 becomes more obvious, probably because this is a more intense ageing test in which early devices fared poorly. To update the Perovskite Database statistics, we added 26 data points from recent high-impact studies from 2021 onwards (Supplementary Table 2). From these data, we can see that in modern studies, 1,000 h operational stability is readily achievable. This higher stability becomes particularly obvious when one realizes that only 4 of the 26 devices decayed to 80% of their original efficiency during stability testing. For the other 22, the number recorded is either the T_{90}, T_{95} or T_{100} lifetime. Indeed, with lifetimes extending well beyond 1,000 h, researchers are turning to accelerated ageing to assess stability, evidenced by the fact that 15 of the 26 devices were tested above room temperature (45 °C to 85 °C).

Panel **c** of the figure compares n–i–p and p–i–n cell stability. Considering cell configuration, we find that (when normalized to ISOS-L1 conditions using a simple acceleration factor model discussed in Supplementary Note 1) there is little difference in stability on average between n–i–p and p–i–n devices, which is surprising, as many state the stability of transport layers in p–i–n

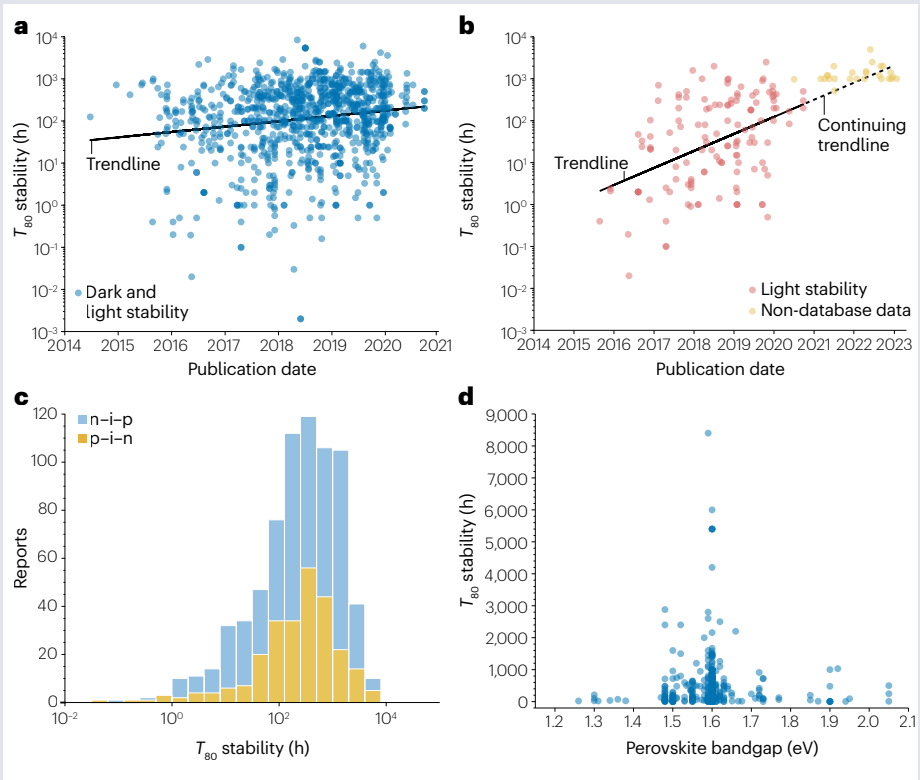

it has been observed that if $\tau > 1$ or $\tau < 0.8$, then the lattice distortion generated induces a photo-inactive, non-perovskite structure to form, normally known as the δ-phase[44].

$MAPbI_3$ has a τ value of ~0.9 and an ideal cubic structure at room temperature. $FAPbI_3$ (τ of ~1) is near the upper boundary for a cubic structure, so it has two phases at room temperature: cubic (α-phase) and hexagonal (δ-phase). High-temperature annealing (>433 K) is required to obtain α-phase $FAPbI_3$ (ref. 45), but δ-phase formation only needs a temperature of ~285 K (ref. 46). Because the δ-phase is more stable than the α-phase, it is difficult to stabilize cubic $FAPbI_3$. By contrast, τ is approximately 0.8 for $CsPbI_3$, which is close to the lower range for the cubic perovskite structure. The thermodynamically stable phase of $CsPbI_3$ at room temperature is the non-photoactive δ-phase, and the photoactive α-phase is obtained by high-temperature annealing of the δ-phase (>633 K)[47].

Perovskite degradation under thermal stress. Some perovskite materials will undergo decomposition reactions under thermal stress. It is important to consider both operational temperatures (−40 °C to 75 °C; a temperature of 65 °C is commonly used as the upper end of PSC operating temperature, but there is evidence that this could be as high as 70–75 °C (refs. 43,48) and temperatures >75 °C for accelerated degradation testing. Note that temperatures used for accelerated ageing should not introduce a new decay mode that would not be observed below 75 °C. $MAPbX_3$ (X = Cl, Br, I) have low decomposition temperatures (<100 °C), with $MAPbI_3$ in particular degrading within the operational range (~60 °C), which is likely to preclude its use as a stable PSC material[49].

The thermal stability of $FAPbI_3$ is reportedly higher than $MAPbI_3$. $FAPbI_3$ films exposed to 150 °C for 60 mins are stable without discoloration, whereas $MAPbI_3$ discolours after ~30 minutes[50]. This enhanced stability is attributed to the stronger interaction between FA_+ and $[PbI_6]^{4+}$ compared with MA^+ (ref. 51). Despite this, $FAPbI_3$ will undergo thermal decomposition at relatively low temperatures (>50 °C), where formamidinium iodide (FAI) decomposes into formamidine and HI[52] (Fig. 3a). Both of these reactions are reversible and in a well-encapsulated device might not be fatal. When the temperature is around 95 °C, formamidine decomposes into *sym*-triazine and ammonia through irreversible reactions[45] (Fig. 3a). When the temperature exceeds the phase transition temperature of α-$FAPbI_3$ (160 °C), $FAPbI_3$ partially decomposes into PbI_2 as FAI evaporates to HCN and NH_3 (ref. 53). This degradation behaviour suggests that $FAPbI_3$ has potential as a stable PSC material between −40 °C and 75 °C, although accelerated ageing above 95 °C is likely to be non-representative.

Because $CsPbI_3$ does not contain volatile and decomposable organic components, it does not break down at low temperatures, and α-$CsPbI_3$ is stable at temperatures as high as 390 °C. Above this, PbI_2 volatilizes and leaves CsI as residue[54]. Hence, accelerated ageing beyond 300 °C is feasible, although the stability of other PSC layers would come into question.

Perovskite degradation under illumination. Ultraviolet and blue wavelengths have the strongest impact on PSC stability[55]. Perovskites rapidly decompose under illumination when oxygen is present, although without oxygen, illumination can still trigger decomposition through simultaneous reversible and permanent reactions[56,57]. Our discussion will focus on illumination without oxygen, assuming high-quality encapsulation.

PbI_2 films degrade into metallic Pb^0 and I_2 gas under simulated sunlight (Xe lamp), with an activation energy (E_a) of ~9 kcal mol^{-1}, or 0.4 eV per Pb atom[58]. The activation energy is increased by a factor of 6 (~57 kcal mol^{-1}) on using a white-light LED. The degradation is retarded completely for photon energies less than 2.3 eV (ref. 59), which is the bandgap of PbI_2, suggesting that degradation is caused by light absorption. For $MAPbI_3$ under a Xe lamp, the E_a for Pb^0/I^2 decomposition is lower than PbI_2 (~6 kcal mol^{-1}) owing to the lower bandgap of $MAPbI_3$ and $[PbI_6]$ octahedral distortion which produces shorter I–I bond distances, aiding the release of I_2 (ref. 58). Moreover, when $MAPbI_3$ is illuminated with energies higher than 450 nm, signals from CH_3NH_2 and H_2 are detected, indicating that the N–H bond in the perovskite can dissociate under sunlight[60] (Fig. 3b). Although most studies examining degradation under illumination have been carried out on $MAPbI_3$, decomposition into Pb^0 has been witnessed in FACs perovskites also[61].

Most perovskites with a >20% Br to I ratio will segregate into I-rich and Br-rich regions under illumination[62]. Considering stability, the funnelling of charges into lower-bandgap (I-rich) regions effectively reduces the maximum V_{OC} of wide-bandgap devices, resulting in a ~10% decrease in V_{OC} over the first hour or so of operation[27,63]. Illumination can also induce a similar process in mixed-cation perovskites in which cations aggregate leading to phase transitions. Density functional theory simulations indicate that cation aggregation in a $FA_{0.89}Cs_{0.11}PbI_3$ perovskite with a uniform distribution of cations can be triggered with relatively little energy (0.133 kJ mol^{-1}) (ref. 64).

Perovskite degradation under bias. In a solar module, partial shading by neighbouring trees, dirt or snow prevents some of the cells from generating photocurrent[65]. Because all cells must pass the same amount of current for the panel to generate power, the cells that are illuminated put the shaded cells into whatever reverse bias is needed for current matching to occur. Cells in reverse bias have both short-term reversible and irreversible degradation problems.

Several interesting observations have been made on the reverse-bias behaviour of perovskite solar cells. When metal electrodes are used, the metal filaments grow all the way through the device under reverse bias to create a shunt[66]. In a reverse-bias current–voltage scan, the current increases very suddenly when the shunt forms, and localized heating is observed with thermal imaging[67,68]. The extreme heating at the shunt causes permanent damage to most layers of the cell. By contrast, this behaviour is not seen when transparent conductive oxides (TCOs) and carbon electrodes are used. In these cells, there is an exponential increase in current that starts typically between −1 V and −4 V when sweeping the voltage to increasing negative values. This current is enabled by the tunnelling of holes from the electron-transport layer due to strong band bending associated with mobile ions redistributing to screen the applied field. After current is passed through a cell in reverse bias for as little as a minute, the efficiency can be reduced by more than 50%. Much, but not all, of this efficiency recovers if the cell is exposed to 1 sun at a positive voltage for approximately 30 minutes. The rapid degradation most likely occurs because the hole density while passing the short-circuit current density in reverse bias is similar to what it would be at the MPP under 1-sun illumination, but the electron density is nearly zero. Consequently, the holes can oxidize iodide more rapidly to form smaller neutral iodine species that can move to interstitial sites, creating a vacancy in the process. With few electrons being present, the reverse reaction is slow. The iodine interstitials act as recombination centres, which greatly reduces the efficiency of the cell. During the recovery process at positive voltage, the iodine interstitials are reduced and return to the octahedral corners. The recovery only

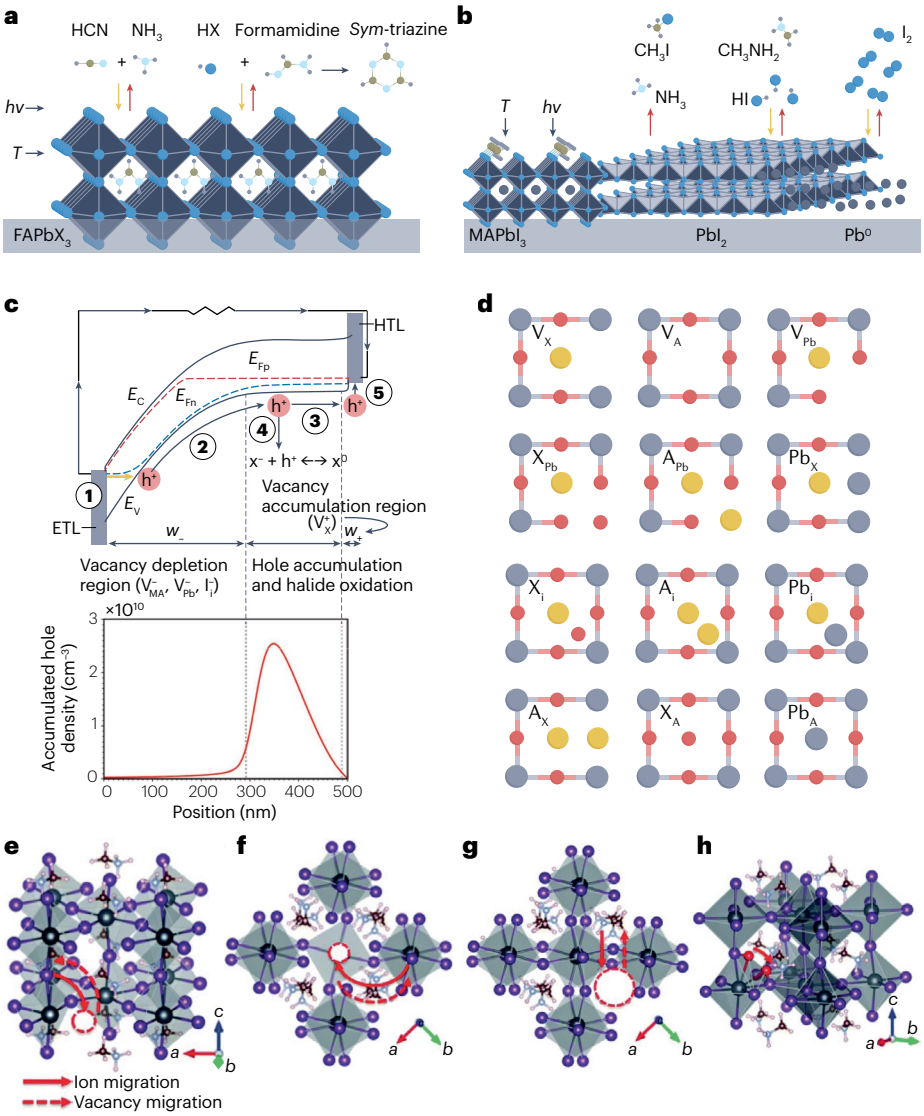

Fig. 3 | Factors affecting perovskite solar cell stability. a, $FAPbX_3$ (X = Br, I or mixed halide) degradation processes under illumination and thermal stress. Processes are indicated by different arrows (red indicates breaking processes and yellow indicates re-forming processes); irreversible processes are indicated by a single red arrow. **b**, $MAPbI_3$ perovskite degradation processes under illumination or thermal (same arrow convention). **c**, Energy diagram of a perovskite solar cell at −3 V showing the main processes occurring in reverse bias. (1) Hole injection: halide vacancies drift towards the hole-transport layer (HTL), resulting in favourable band energetics for hole injection via trap-assisted tunnelling at the interface between the electron-transport layer (ETL) and perovskite. (2) Hole drift: a strong electric field pulls the holes away from the space charge region. Holes accumulate at the edge of the region where there is no net electric field. (3) Hole diffusion: a high concentration gradient of holes in the bulk results in diffusion of the holes towards the HTL. (4) Halide oxidation by holes: part of the holes that build up in the perovskite bulk oxidize halides into neutral halogens. (5) Hole extraction into the HTL. In this band diagram, E_C and E_V are the perovskite conduction and valence bands, respectively. E_{Fn} and E_{Fp} are the hole and electron quasi-Fermi levels, respectively. W_- and W_+ are vacancy depletion region and vacancy accumulation region, respectively. Below is the distribution of the holes injected by surface-state-assisted tunnelling and accumulating close to the edge of the vacancy-depleted region at reverse bias for a tunnelling current of 0.3 mA cm^{-2}. **d**, The 12 types of native point defects found in metal-halide perovskites. **e**–**h**, Diffusion paths for V_I (panel **e**), V_{MA} (panel **f**), V_{Pb} (panel **g**) and I_i (panel **h**) defects. Panel **a** reprinted with permission from ref. 52, RSC. Panel **b** reprinted from ref. 58, CC BY 3.0. Panel **c** reprinted with permission from ref. 67, Wiley. Panel **d** reprinted from ref. 75, Springer Nature Limited. Panels **e**–**h** reprinted with permission from ref. 76, RSC.

occurs, however, if the iodine species stay in the perovskite film. For this reason, internal barriers that confine the iodine to the perovskite are critically important.

If strategies for preventing degradation in reverse bias are not found, then engineering solutions for preventing degradation due to partial shading will be needed. In silicon solar panels, strings of cells are protected by a few bypass diodes that are located in the junction box. The current can be routed to the diodes through metal ribbons. The approach could be used relatively easily in panels made with perovskite–silicon tandems[69]. The breakdown voltage of the tandem is the sum of the breakdown voltages of the subcells. Many tandems can be protected by one bypass diode because of the high breakdown voltage of silicon. It is not clear, however, how to use bypass diodes in thin-film panels in which cells with a length greater than a metre are separated from each other by laser scribes. If one of these cells were shaded, some of the current would have to travel as far as the length of the cell to get to the bypass diode on the edge of the panel and then travel back. One of the electrodes would probably be a TCO, and the voltage drop over such a large distance would be excessive. It is for this reason that bypass diodes are typically not used in commercial CdTe solar panels.

It is quite possible that the degradation in reverse bias is similar in nature to what happens under 1 sun at the MPP in good solar cells that do not have weaknesses associated with poor packaging, mobile additives or reactive electrodes. Because degradation in reverse bias is approximately 100,000 times faster, it might offer an excellent way to test new materials and processing conditions rapidly to assess their impact on stability. In particular, reverse biasing can be used to generate mobile iodine in order to assess barrier quality (Fig. 3c).

Effect of defects on PSC stability. A large number of defects are generated during perovskite crystallization. Defect densities >10^{14} cm^{-3} have been reported for optimized perovskite thin films[70], most of which appear at surfaces and grain boundaries. Perovskite composition and

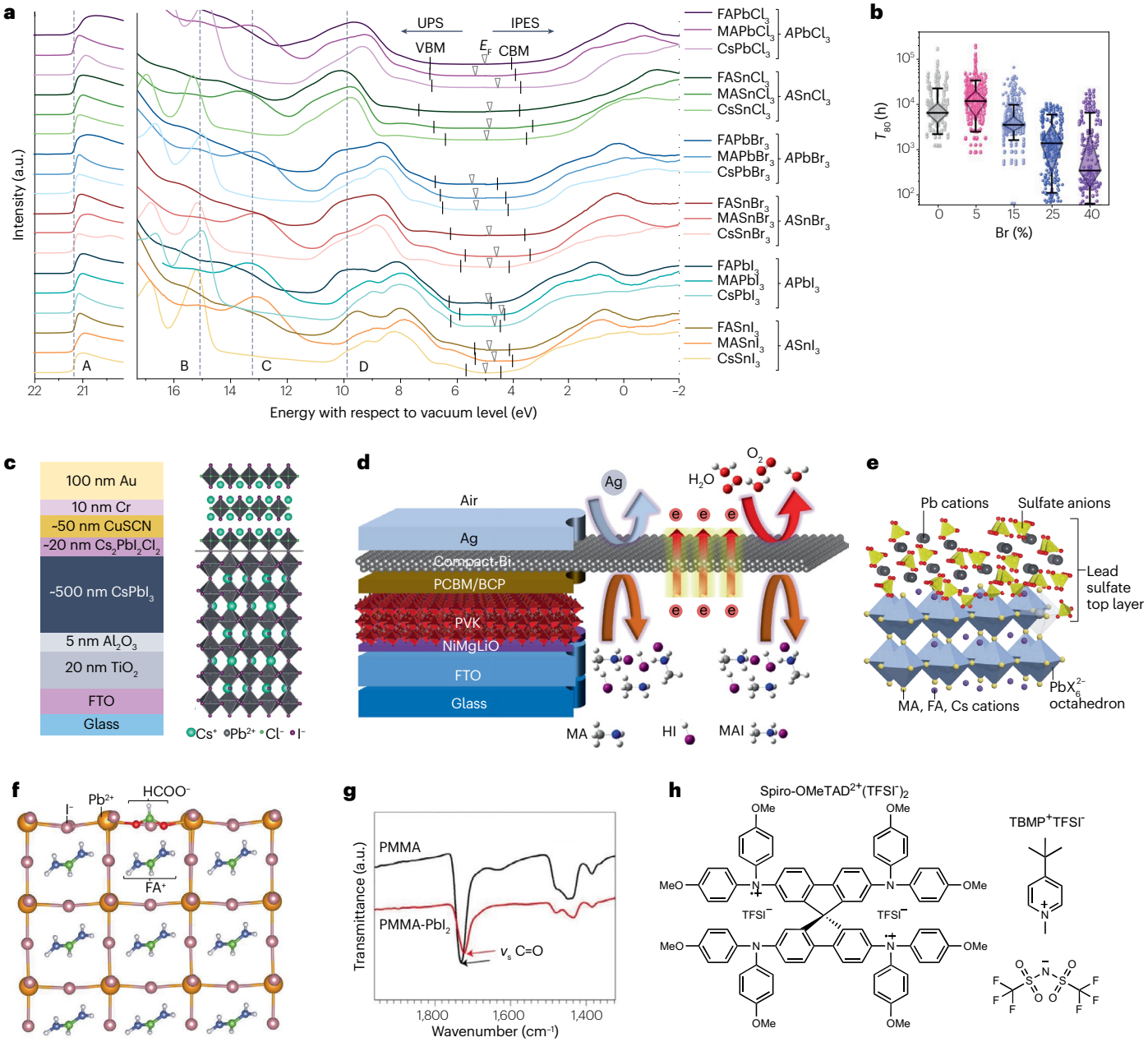

fabrication conditions have a substantial influence on defect type and concentration[71]. The primary defects affecting PSC performance are point defects at grain boundaries or surfaces[72], including antisites (MA_{Pb}, MA_I, Pb_{MA}, I_{MA} and I_{Pb}), interstitials (MA_i, Pb_i and I_i) and vacancies (V_{MA},V_{Pb} and V_I)[73] (Fig. 3d). MHPs are defect-tolerant materials, but even shallow defects can lead to non-radiative recombination and reduce V_{OC}, albeit to a much lesser extent than traditional semiconductors. More important to stability, defects aid ion migration, meaning that defects migrate[74] (Fig. 3e–h), accumulate and propagate leading to irreversible degradation[75].

Calculations of ion migration activation energies find that halide ions contribute the most to ion migration (5 times as much as MA or Pb, for example[76]). Ion migration energies vary due to measurement, perovskite composition, defect densities and PSC fabrication, but values between 0.1 eV and 0.9 eV have been reported[10,77–79]. Typically, these values are calculated as a function of temperature only, but ion migration is governed by temperature and illumination. For example, ion migration activation energy has been observed to decrease substantially (0.29 eV to 0.1 eV) when films are under low-intensity illumination (10 mW cm^{-2}) (ref. 80).

Defects also collect and trap carriers, inducing irreversible degradation of perovskite[81,82]. Two deep-level trap bands, I (0.27 eV) and II (0.36 eV), have been observed in iodine-based PSCs, which correspond to iodide interstitials (I_i^- and I_i^+). Under reverse bias, a trap-filling process occurs between I_i^- and the injected holes (h^+) to form I_i^0. I_i^0 can be oxidized to I_i^+ by valence band oxidation[83] or can form I_2 through a bimolecular reaction, which induces iodide loss and leads to irreversible degradation[67,84].

Fig. 4 | Strategies for stable perovskite solar cells. a, Effect of A cations on the valence band maximum (VBM) and the conduction band minimum (CBM) of different perovskite systems, obtained from ultraviolet photoelectron spectroscopy (UPS) and inverse photoemission spectroscopy (IPES) spectra. For better comparability, the curves are offset vertically, and the high-energy cut-offs are aligned at the excitation energy of 21.22 eV, marked by line A. Lines B, C and D indicate characteristic features in the density of states, corresponding to the position of Cs, MA and FA related states, respectively. The extracted positions of VBM and CBM are given by black vertical markers, and the Fermi level positions are marked by triangles. **b**, T_{80} lifetime statistics for mixed-cation, mixed-halide perovskite film with different Br concentrations. Each Br concentration contains results from 32 different cation compositions. Films were tested at 65 °C and 1-sun illumination. **c**, A perovskite solar cell (PSC) using a 2D $Cs_2PbI_2Cl_2$ layer atop the 3D perovskite active layer. **d**, PSC using a Bi interlayer and schematic of its shielding capability, prohibiting both inward and outward permeation. **e**, Schematic illustration of perovskite films protection through in situ formation of a lead sulfate top layer on the perovskite surface. **f**, Calculated crystal structure illustrating the passivation of an I^- vacancy at the $FAPbI_3$ surface by a $HCOO^-$ anion. All chemical species are shown in ball-and-stick representation. Pb^{2+}, yellow; I^-, pink; oxygen atoms, red; carbon, green; nitrogen, blue; hydrogen, white. **g**, Fourier-transform infrared (FTIR) spectra of PbI_2·PMMA prepared by mixing polymethyl methacrylate (PMMA) with PbI_2 in a molar ratio of 1:1, and the pristine PMMA films. The arrows indicate the stretching vibration peak of C=O in the two films. This shift in FTIR signal indicates the existence of a C=O, PbI_2 adduct that regulates crystallization. **h**, Illustration of an ion-modulated radical doping strategy for spiro-OMeTAD developed by Gao et al.[168]. FA, formamidinium; FTO, fluorine-doped tin oxide; MA, methylammonium; PCBM, phenyl-C_{61}-butyric acid methyl ester; PVK, perovskite; TCO, transparent conductive oxide; TFSI, bis(trifluoromethanesulfonyl)imide. Panel **a** reprinted from ref. 98, CC BY 4.0. Panel **b** reprinted from ref. 22, Springer Nature Limited. Panel **c** reprinted with permission from ref. 10, AAAS. Panel **d** reprinted from ref. 128, CC BY 4.0. Panel **e** reprinted with permission from ref. 80, AAAS. Panel **f** reprinted from ref. 105, Springer Nature Limited. Panel **g** reprinted from ref. 155, Springer Nature Limited. Panel **h** adapted with permission from ref. 168, AAAS.

Effect of metal electrodes on PSC stability

Most highly efficient PSCs use a metal top electrode; gold is the most-used electrode in n–i–p devices, but copper or silver is more common for p–i–n devices. Metal electrodes are easily corroded by halides that migrate from the perovskite layer, which reduces conductivity over time. Furthermore, metal ions generated by corrosion can migrate into the perovskite, accelerating PSC degradation[85]. For example, iodide on perovskite film surfaces can diffuse through CTLs to the surface of a silver electrode. The ions react with silver and form silver iodide (AgI), an insulating layer that hinders charge transport[86]. The opposite is also possible. Au^- can migrate through spiro-OMeTAD into the perovskite layer under 70 °C annealing to induce perovskite degradation[87]. It is believed that under illumination, the ion migration in perovskites is reversible and does not cause permanent degradation. However, when ions, especially halides, migrate to a metal electrode and react, this causes irreversible degradation[88].

Effect of charge-transport layers on PSC stability

For highly efficient PSCs, charge-transport layers (CTLs) are indispensable. Any physical or chemical alteration of the transport layer material, the perovskite–CTL interface[89] or the CTL–electrode interface can affect the long-term stability of PSCs[90].

For example, TiO_2, a common electron-transporting material in n–i–p PSCs, has abundant oxygen vacancy defects (Ti^{3+} sites, especially at the surface) that are effectively deep electron-donating sites. In the presence of ultraviolet light, iodide ions at the perovskite–TiO_2 interface can be oxidized into iodine, resulting in the decomposition of the perovskite[91]. NiOx and poly(3,4-ethylenedioxythiophene) polystyrene sulfonate (PEDOT:PSS) can undergo photo- or chemical reactions with lead halides. By contrast, pentathienoacene (PTA) and polybisphenyl(trimethylphenyl)amine (PTAA) seem inert to lead halides[92]. Currently, spiro-OMeTAD-based PSCs hold the record for single-junction PSC efficiency. Pristine spiro-OMeTAD has intrinsically low hole mobility. As such, it is necessary to increase the hole mobility by adding additives, with the most-used additives being lithium bis(trifluoromethanesulfonyl)imide (Li-TFSI) and *tert*-butylpyridine (*t*BP)[93,94]. Although Li-TFSI and *t*BP improve PSC performance, they also bring challenges to long-term stability: *t*BP can corrode the perovskite layer through reaction with PbI_2, and Li^+ in Li-TFSI can diffuse into the perovskite interior and decompose the perovskite structure[95–97].

Strategies for stable PSCs

Several stability-enhancing strategies have been developed, such as increasing ion migration energies and crystal stability through alloying, protecting the perovskite and CTLs from external stressors and passivating interfacial defects using barrier layers, decreasing defect density and suppressing ion migration using functional additives, and using robust CTLs (Figs. 4 and 5).

Perovskite phase stabilization

A-cation alloying. The A site in the perovskite crystal structure does not directly affect the band edge states as these states are formed from Pb and halide orbitals. It does, however, affect the bandgap indirectly through changes to octahedral tilting or distortion of the MX_6 framework, which changes the B–X bond length and induces VBM and CBM changes[98,99] (Fig. 4a). Indeed, as the size and geometry of the A cation affects the bond length and bond angle of the perovskite crystal, it has great influence on the crystal stability and the electrical properties of the perovskite.

$FAPbI_3$ has a narrower bandgap (1.48 eV) than that of $MAPbI_3$ (1.6 eV) (Fig. 4a), so $FAPbI_3$-based perovskites are preferred as their bandgap is closer to optimal for maximum device efficiency (1.34 eV)[100]. Indeed, the majority of high-efficient PSCs are $FAPbI_3$-rich recipes. However, as the tolerance factor for $FAPbI_3$ is close to 1, $FAPbI_3$ will naturally lose its cubic phase at room temperature. To stabilize α-$FAPbI_3$, partial replacement of FA^+ with smaller-radii cations (MA^+, Cs^+, Rb^+) is used. The introduction of MA^+ enables the perovskite to obtain its α-phase at a lower temperature than pristine $FAPbI_3$ (ref. 101), but is generally thought to decrease the light and thermal stability of $FAPbI_3$ perovskite as MA^+ is more volatile than FA^+ (ref. 102). Counterintuitively, up to ~10% MA incorporation has been shown to improve stability[22,103].

Partially replacing FA^+ with smaller-radii cations such as Cs^+ not only stabilizes α-$FAPbI_3$ but also improves thermal stability due to the strong chemical bonding between Cs^+ and $[PbI_6]^{4+}$. $Cs_{0.1}FA_{0.9}PbI_3$ has shown better photo- and moisture stability than $FAPbI_3$. This stability is attributed to the introduction of Cs^+, which shrinks the perovskite crystal cubo-octahedral volume and increases the A-site-I bond energy[102]. To further improve stability, complex mixed-cation systems have also been explored, such as CsMAFA and RbCsMAFA. Adding more elements increases the entropy of mixing to stabilize the perovskite phase[40,104].

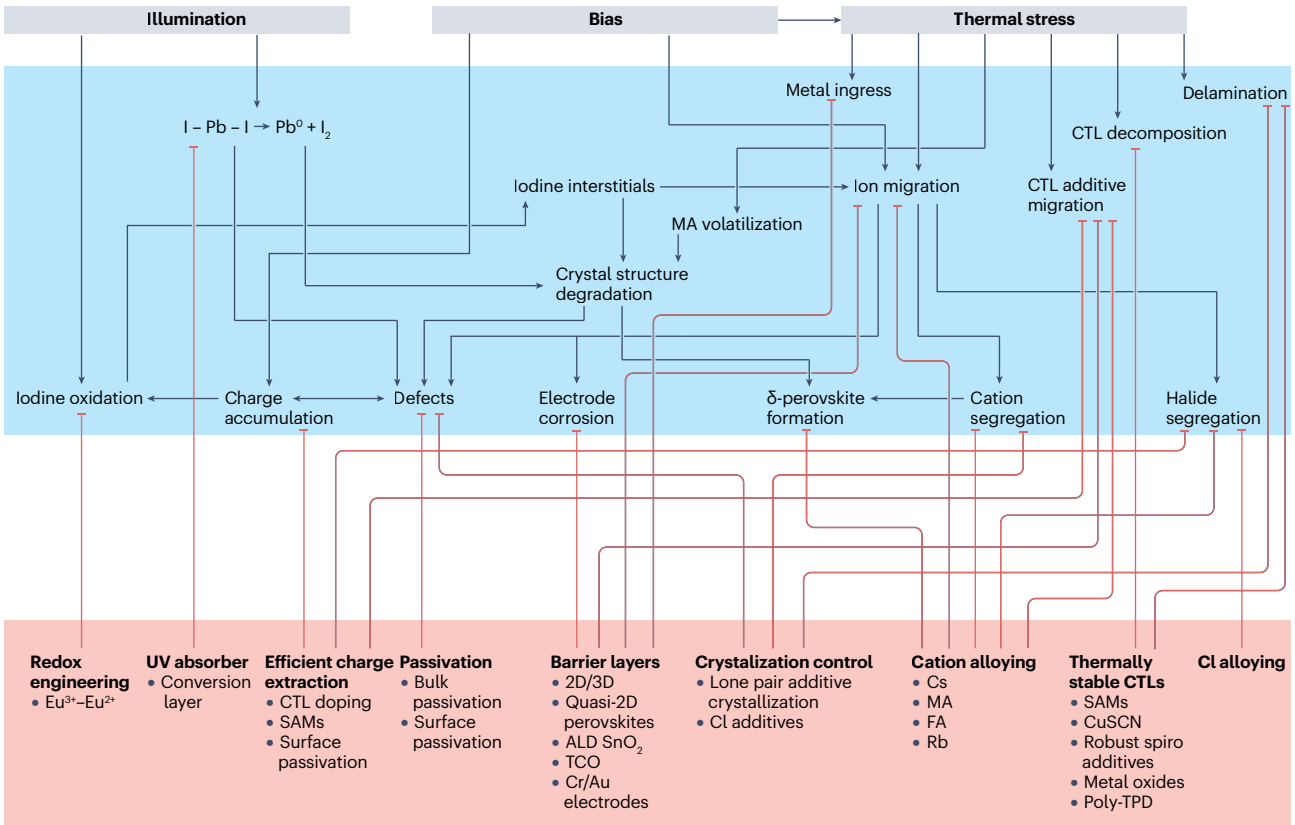

Fig. 5 | Overview of perovskite solar cell stability. The grey boxes represent causes and the blue box effects. The red box represent mitigation strategies and specific implementations. 2D/3D, 2D/3D heterostructure solar cell; ALD, atomic layer deposition; CTL, charge-transport layer; CuSCN, copper thiocyanate; FA, formamidinium; MA, methylammonium; poly-TPD, poly[*N*,*N*′-bis(4-butylphenyl)-*N*,*N*′-bis(phenyl)benzidine]; SAMs, self-assembled monolayers; spiro, 2,2′,7,7′-Tetrakis(*N*,*N*-di-*p*-methoxyphenylamine)-9,9′-spirobifluorene; TCO, transparent conductive oxide.

Various other methods to stabilize α-$FAPbI_3$ have been discussed in the literature (for example using pseudo-halides[105] or using methylenediammonium[38] or isopropylammonium[106] as additives). For many of these, it is unclear whether perovskite alloying has occurred. Including a small amount of Cs^+ or MA^+ to stabilize $FAPbI_3$ results in a non-cubic perovskite crystal structure with an octahedral tilt of ~2° at room temperature[107]. This α-phase stabilization is not exclusive to alloying additives, as it can also be achieved by additives at the perovskite grain boundaries. Moreover, if alloying cations are unevenly distributed, nanoscale local regions of perovskite can lose their 2° tilt, forming regions of hexagonal polytypes that expand over time, and resulting in δ-phase formation[107]. Increasing the annealing temperature or the annealing time results in more homogenous mixing of A-site cations and higher PSC stability[108].

Introducing large-radius cations such as PEA^+ or BA^+ into $FAPbI_3$ perovskite is another important strategy to improve perovskite stability[109]. The exchange of large-radii cations leads to the collapse of the 3D perovskite crystal structure and the introduction of a quantum-confined, usually 2D structure[110]. If large A cations are mixed directly into the perovskite precursors, then a mixed, quasi-2D film containing various thicknesses of 2D and quasi-2D perovskite tends to form. This mixed film has enhanced stability due to an increased hydrophobicity and the presence of large-cation layers hindering ion transport, but lower efficiency due to an increased bandgap, decreased mobility and higher exciton binding energies[111]. Applying 2D perovskite atop the bulk 3D to passivate the surface and block ion transport out of the cell can be used to remediate these issues.

A summary of operational stability enhancements from A-site alloying is found in Supplementary Table 3.

X-anion alloying. Unlike the A-site cation, the X-site anion directly contributes to the band edge of the perovskite. Replacing I^- with Br^- or Cl^- can tune the bandgap, regulate perovskite grain growth and improve the chemical stability of perovskite films. Partially replacing I^- with Br^- can suppress the δ-phase formation of FA-rich or Cs-rich perovskites[112,113], and perovskites with 5% Br have shown better T_{80} stability[22] (Fig. 4b).

The introduction of Cl^- into perovskite precursors can substantially improve the quality, morphology[114] and crystallinity of majority iodine perovskites, although whether Cl alloys into the perovskite is still debated and probably depends on various factors[115]. Introducing MACl into $FAPbI_3$ perovskite is one of most popular methods to prepare stable α-$FAPbI_3$ films[116], as the Cl-containing perovskite system is more thermodynamically stable and the introduction of MA shrinks the volume of the $FAPbI_3$ crystal, which also improves the stability of the perovskite structure[117]. In wider-bandgap perovskites that contain

important amounts of Cs and Br, the lattice parameters are smaller, and more chlorine can be incorporated on the X site[118]. These compounds are more stable against light-induced phase separation.

All-inorganic perovskites. All-inorganic perovskites $(Cs,Rb)Pb(I,Br)_3$ are more thermally stable than their hybrid counterparts. Because the bandgaps of all-inorganic perovskites are wider than those of FA-based perovskites, they are typically considered for tandem applications. The narrowest bandgap available is for $CsPbI_3$ (~1.7 eV), which is well matched for Si/perovskite tandems. Like for $FAPbI_3$, the photoactive phase of $CsPbI_3$ is difficult to maintain at room temperature. Many strategies have been developed to stabilize α-$CsPbI_3$: A-cation alloying, X-anion alloying and additive engineering. For example, 18-crown-6 ether has been used as an additive to stabilize the cubic phase of $CsPbI_3$, and devices maintained ~91% of their initial PCE after 1,000 h in N_2 at 85 °C (ref. 119). Polyvinylpyrrolidone (PVP) has likewise been used, with PSCs showing no visible decrease in PCE after 3,500 h at 35 °C, and decreasing by only 20% after 2,100 h under continuous illumination at 110 °C (ref. 10) (Fig. 4c).

Although highly thermally stable, all-inorganic PSCs tend to suffer from lower efficiencies than their hybrid counterparts. These lower efficiencies have been attributed to high defect densities induced by fast crystallization, resulting in short carrier lifetimes and low photoluminescent quantum efficiency[120]. To improve efficiency, dimethylammonium has been used to stabilize the β-phase $CsPbI_3$ and to control perovskite crystallization[121], and surface treatments have been used to reduce surface defect densities[120]. Using a CsF surface treatment, an all-inorganic PSC with a 1.74-eV bandgap achieved 21% PCE[122], ~75% of the thermodynamic limit. The highest-performing hybrid perovskites can achieve >80% of this limit[123], so there is some room for improvement. The carrier lifetimes recorded for these all-inorganic films are roughly one-quarter that of the highest-performing hybrid films (~700 ns compared with ~2,900 ns), suggesting that defect densities can be further reduced.

Barrier layers for stable PSCs

Barrier layers are thin layers deposited at interfaces within a PSC to improve efficiency and stability. These layers can protect from external stressors (such as moisture or ultraviolet light), passivate interface defects, block ion migration and inhibit interfacial chemical reactions[124].

CTL–electrode interface barrier layers. The main function of a barrier layer at the CTL–anode interface is to block the migration of perovskite and metal ions crossing the interface without reducing conductivity. There are various barrier layers in use (metal oxides[125], graphene[126] and organic self-assembled monolayers (SAMs)[127]). An illustrative example is Au or Ag infiltration in PSCs aged at high temperature. Introducing 10 nm of chromium between a Au anode and the HTL entirely mitigates Au infiltration into the perovskite layer after 75 °C ageing under light, suggesting that Cr is an effective barrier to metal ion migration[87]. Alternatively, bismuth interlayers can protect metal electrodes from iodine corrosion or perovskite ingress, preventing all detectable Ag infiltration into the perovskite layer after ageing at 85 °C for 100 h under light. Bismuth-protected devices maintain 95% and 97% of their initial PCE after 500 h under 85 °C and light soaking conditions, respectively[128]. TCO electrodes such as indium tin oxide or indium zinc oxide can also reduce ion infiltration and increase stability. The most effective TCO layers are fabricated by sputter deposition, but high-energy sputtering can easily damage other layers. Atomic layer deposition (ALD) can remediate this issue as has been demonstrated with SnO_2 in both perovskite tandems and single-junction devices[129]. SnO_2 can act as a barrier layer in its own right, or in conjunction with a sputtered TCO layer[130].

Alternatively, one can replace metal electrodes with carbon electrodes to avoid degradation due to electrode corrosion or metal ion migration. Interface barrier layers are often used to improve the contact or energy-level alignment between the carbon electrode and the perovskite layer, partially offsetting the efficiency decrease caused by the carbon electrode[131].

Perovskite–CTL interface barrier layers. The high surface defect density of perovskite films accelerates degradation while corrupting other layers through ion migration. Barrier layers that can passivate surface defects and block ion migration are highly attractive. Various materials have been demonstrated as perovskite–HTL interface barrier layers, including 2D materials[132], quantum dots[133], metal oxides[134,135], functional polymers[136], small molecular compounds[137,138] and ammonium salts[139,140]. The most popular passivation/barrier layer in modern PSCs is a layer of 2D perovskite, with several reports of good operational stability at ≥60 °C in 2022 alone[9,10,141,142]. For example, pure-phase 2D perovskite single crystals dispersed in acetonitrile were coated onto 3D perovskite to form a highly controllable 2D/3D interface. An advantage of 2D perovskite is its relatively high conductivity compared with other insulating barrier layers, meaning that layers up to 80 nm in thickness have been used without resistive losses[143]. Using a conformal 50-nm-thick 2D layer, devices with >23% PCE were fabricated, which also demonstrated T_{99} > 2,000 h following the ISOS-L1 (MPP, 60 °C) protocols, a large increase compared with control devices (T_{80} of ~500 h)[9] (Fig. 4d). Depositing CsCl onto $CsPbI_3$ has been used to form an all-inorganic 2D/3D heterostructure (Fig. 4c). This strategy increased the barrier to ion migration in PSCs by a factor of 2 and increased the T_{80} stability (ISOS-L3) by a factor of ~3 at 110 °C to >2,000 h. Device stability was measured at several temperatures and used to extrapolate the T_{80} lifetime at 35 °C to be ~5 years[10].

Using non-2D perovskite barrier layers, such as inorganic lead sulfate, also leads to impressive stability results. For example, although the ion migration energy of control devices is ~0.1 eV, no transition to ionic transport was observed in lead-sulfate-capped PSCs below 55 °C (Fig. 4e). Using this technique produced >20% PCE cells with a T_{97} > 1,000 h at 65 °C (ISOS-L3)[80]. In addition, hybrid material ferrocenyl-bis-thiophene-2-carboxylate ($FcTc_2$) strongly binds to the perovskite surface and effectively prevents surface MA^+ from escaping the film under light (1 sun) and heat (85 °C). Devices with PCE ~24% exhibited a T_{98} of 1,500 h (ISOS-L1, room temperature)[144].

Additive engineering

Perovskite grain boundaries and surfaces are vital to the stability of PSCs as they contain the majority of defects, and these defects tend to propagate over time[15,145]. Reducing the density of defects at grain boundaries inhibits degradation and ion migration. Both functional materials and solvent additives can regulate crystallization to increase grain size and passivate grain boundaries[146]. This section investigates the effects of salts and organic compound additives on PSC stability.

Additive salts. A popular set of additives are organic ammonium halide salts. These additives exist in different formations at perovskite grain boundaries and surfaces. Some ammonium species form

low-dimensional perovskites, which improve PSC stability by inhibiting ion migration[147,148]. Alternatively, organic cations with large molecular volumes, such as $NH_3I(CH_2)_8NH_3I$, cannot form low-dimensional perovskite but can heal surface defects through hydrogen bonding, X-site vacancy passivation (halogens) and NH_3 groups binding to A-site vacancies or Pb–X antisite defects[2,149].

Ionic liquids (ILs) are increasingly used to improve the stability of PSCs through three mechanisms[150]. First, the ionic liquid reacts with PbI_2 to form an intermediate complex, which increases the activation barrier to perovskite nucleation growth, thus increasing grain size and reducing grain-boundary density. Next, the formation of hydrogen bonds between the ionic liquid and MA^+ or FA^+ inhibits relevant ion migration, thereby increasing PSC stability. Finally, ionic liquids have various functional groups that can passivate different perovskite surface defects, suppress ion migration and retard lead oxidation and the compositional segregation of perovskites. Formamidinium formate (FAHCOO) was used to fabricate >25% PCE PSCs with a T_{80} of 400 h (compared with 150 h for control devices)[105] (Fig. 4f).

Organic compounds as additives. Organic compounds are some of the most commonly used perovskite additives. These materials contain N-donor, S-donor or O-donor groups. The electron lone pair of these groups can react with lead halide precursors to form complexes that, similarly to ionic liquids, retard the nucleation rate of perovskites and reduce the density of grain boundaries[151]. Concurrently, these electron donors effectively passivate perovskite defects, thereby improving the stability of PSCs. Some oligomer additives can also be used as linkers between grains to improve grain-boundary stability[152]. Besides the above functions, conjugated organic additives can modify energy-level alignment to promote carrier extraction at interfaces, inhibiting the accumulation of charges and improving stability[153,154].

A notable example is PMMA, which contains C=O functional groups. When PMMA is added to a perovskite precursor solution, an intermediate adduct is formed between C=O and PbI_2 (Fig. 4g). The intermediate adduct formation effectively regulates the crystallization process of the perovskite and increases the perovskite crystal size considerably[155]. As another example, the theophylline molecule contains N–H and C = O functional groups. The N–H groups can form a hydrogen bond with iodine and assist the interaction of C=O with antisite Pb (lead) defects on the perovskite surface leading to suppressed ion migration, devices with theophylline showing better stability under operation[156].

It should be noted that there is currently no standard for evaluating which type of additive is better, nor is there any authoritative comparative study indicating additive hierarchy. At present, there is consensus in the field of PSCs that materials containing S, N, O or P atoms can form adducts through Lewis acid–base reactions with lead atoms, which regulate perovskite crystallization and reduce defects in perovskite films[151,157]. However, how best to compare the efficacy of different additives remains a problem for the field.

Robust transport materials and relevant additives for stable PSCs

For p–i–n PSCs and p–i–n-based tandem devices, the most commonly used HTLs (PTAA, NiOx and SAMs) have shown good stability[37,158], and ALD SnOx as ETL can show good stability and high efficiency. For n–i–p devices, SnO_2 seems to effectively solve the instability induced by TiO_2 (ref. 159), but resolving the instability induced by spiro-OMeTAD while ensuring higher efficiency is a challenge[160–162]. Here we highlight work on improving the stability of spiro-OMeTAD and on the development of additive-free HTMs, as many HTM additives cause degradation when they diffuse into the perovskite.

PSCs with record efficiency have consistently been fabricated in the n–i–p structure. Spiro-OMeTAD is the best-performing HTM for these cells in terms of efficiency, but it requires dopant additives to increase its mobility, and stability problems caused by additives in spiro-OMeTAD have resulted in consistently poor stability from record devices (Fig. 2c). To solve or offset the negative effects of spiro-OMeTAD additives, several strategies have been used, including reducing the use of additives[163], introducing Li^+ complex agents to inhibit Li^+ migration[164,165], introducing substances with hydrophobic groups[166] and developing new doping regulators[167]. For example, stable organic radicals have been used as dopants along with ionic salts as doping regulators to oxidize spiro-OMeTAD and increase its hole mobility (Fig. 4h). The efficiency of devices made using this method exceeded 25% PCE, with the T_{80} of unencapsulated devices aged at 70 °C (measured in an N_2 glovebox) increasing from ~264 h to ~796 h (ref. 168).

Many researchers are focused on the development of additive-free HTMs, including organic small-molecule materials[93,169], polymers[170] and inorganic hole-transport materials[171]. For example, PSCs using compact, conformal CuSCN as a HTL have recorded PCEs exceeding 20% and show excellent stability at 60 °C over 1,000 h (ref. 172). Furthermore, the efficiency of additive-free, polymer-HTL-based PSCs has exceeded 24% and maintain 80% original efficiency after ~1,000 h under 1-sun irradiation (white LED, 100 mW cm^{-2}, 25 °C, under N_2)[173].

Accelerated lifetime testing

It is impractical to use decades-long protocols for stability testing. Hence, correlation between accelerated testing protocols, degradation models and real-world outdoor testing were used to establish the IEC standards used to certify Si PV panels[174]. These standards do not extend to perovskite PV as the acceleration factors used to correlate simulated and real-world testing are different[35]. Additionally, perovskite PV demonstrates behaviour unknown in Si PV related to ion migration and electrochemistry, such as performance recovery under dark conditions[175,176].

There are two purposes to stability testing. The first is to identify the rough operational stability of a device in comparison to a control or another study – this type of reporting is common across PSC research. The second is to identify the failure modes of devices and to develop a model for how devices degrade with time. Considering that many PSCs have been reported with little to no degradation under ISOS-L1 conditions for >1,000 h (refs. 9,141,177), accelerated testing and modelling of degradation modes is becoming ever more important. This concept has been used successfully in organic photovoltaics (OPV) and in Si PV where degradation is assumed to derive from a set of individual activation energies that interact multiplicatively[178], but has seldom been used in perovskite PV.

In OPV and Si PV, thermally induced decay is modelled using the Arrhenius equation, to which light intensity is simply assumed to apply multiplicatively. For example, for an arbitrary decay function with some number of constant decay rates k,

$$\mathrm{PCE}(t) = f(k_1, k_2, k_3, \ldots, t) + C$$

where each decay rate represents a different decay mode in the material (such as halide migration, cation diffusion or B-site oxidation). Traditional models use

$$AF = \frac{k_{acc}}{k_{ref}} = e^{\frac{E_a}{k_B}\left(\frac{1}{T_{ref}} - \frac{1}{T_{acc}}\right)}$$

as the acceleration factor for thermal degradation, where E_a is the activation energy for thermal degradation, and T_{ref} and T_{acc} are reference and elevated temperatures, respectively[178]. To include light intensity, a factor is multiplied such that

$$AF_{L+T} = AF_L AF_T = \frac{I_{acc}}{I_{ref}} e^{\frac{E_a}{k_B}\left(\frac{1}{T_{ref}} - \frac{1}{T_{acc}}\right)}$$

where I_{acc} and I_{ref} represent the light intensity of accelerated and reference testing, respectively. Depending on the decay mode, one might find that only some decay rates are affected by heat and others by illumination intensity[10]. For example, a simple model for N_2-encapsulated $CsPbI_3$ PSCs that considers only one light intensity has been reported. The PCE of devices with and without a 2D capping layer degraded according to a biexponential relationship, with two decay rates. Interestingly, both decay rates followed the same relationship with temperature, so were both derived from the same activation energy. Fitting data to this simple model found good agreement, and the lifetime of cells operated at 35 °C could be predicted to be >5 years (Fig. 6a,b). This result is even more impressive when considering that these cells were under constant 1-sun illumination, which is roughly 5 times the average irradiation experienced by a typical real-world panel, suggesting a similar lifetime to that of established PV technology[25].

An interesting finding from this work is that the common fast initial decay, often classified as 'burn-in', could be generated by the same mechanism that causes slow long-term decay. What is still unclear, however, is why ion migration has two different decay modes and to what extent each of them is reversible.

A more comprehensive model for $MAPbI_3$ that includes humidity, oxygen, light intensity as well as temperature has been developed[179]. In this model, the light intensity acceleration factor is $(I_{acc}/I_{ref})^{0.7}$, so less important than the linear multiplicative factor used for established PV, but still indicates that high light intensities could substantially speed up degradation testing. Little work has been done on accelerated testing using high light intensities, although two reports demonstrate stability up to 10-sun intensity (T_{90} ~ 150 h, Fig. 6c) suggesting this could be a useful parameter to accelerate testing timescales[180–182].

Another key consideration when selecting accelerated testing scenarios is the effect of cycling ageing conditions as, in real-world use, a large discrepancy between light-cycled devices (12 h light, 12 h dark) and continuously illuminated devices will occur. For example, in one study, a light-cycled device yielded an average efficiency of 96% initial PCE across 250 h, compared with a continuously illuminated cell that averaged only 88% initial efficiency (Fig. 6d). In the same study, temperature-cycled devices (65 °C to −10 °C every 2 h) degraded at a rate in between devices held at either −10 °C or 65 °C (ref. 175). Monitoring the performance of a device subjected to simulated weather conditions from two days of each month in the year resulted in several interesting observations. Over the course of each day, the PSC degraded substantially relative to what was expected from single MPP measurements at each light intensity and temperature. Initially, the degradation was reversible and the device completely recovered by the second day, but the proportion of reversible decay reduced over time, and after the first week most degradation was irreversible. Exposure to high light intensities seemed to dominate PSC degradation rather than high temperatures. Understanding what causes reversible and irreversible change to PCE is a pertinent question for future testing. Even this small pool of results suggests that many different testing conditions need to be applied, modelled and compared to build up a reliable testing protocol.

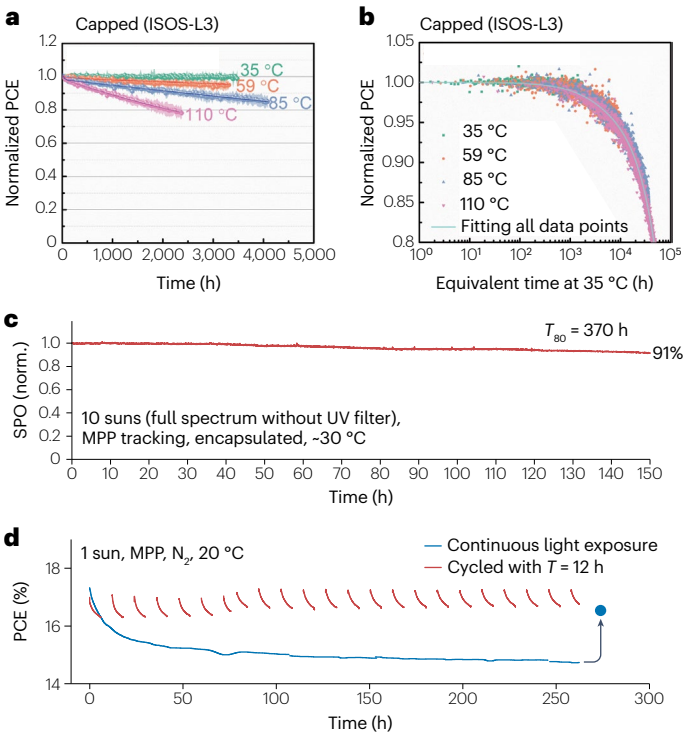

Fig. 6 | Accelerated ageing. a, Results from accelerated ageing at different temperatures for $CsPbI_3$ all-inorganic perovskite solar cells (PSCs). **b**, Modelling these data using an Arrhenius factor fitting to calculate an acceleration factor, suggesting that the cell aged at 35 °C should have a T_{80} > 5 years. **c**, Maximum-power-point (MPP) tracked PSC data at 10-sun intensity using a fluorine-doped tin oxide/SnO_2/phenyl-C_{61}-butyric acid methyl ester/$FA_{0.83}Cs_{0.17}PbI_{2.7}Br_{0.3}$/polybisphenyl(trimethylphenyl)amine/Au structure. **d**, Data comparing MPP-tracked PSCs using constant 1-sun intensity and light cycling. The light-cycled device produced 96% of its initial efficiency on average throughout the 250-h test, whereas the device under constant illumination produced only 88% of its initial efficiency on average. PCE, power conversion efficiency; SPO, stabilized power output. Panels **a** and **b** reprinted with permission from ref. 10, AAAS. Panel **c** reprinted from ref. 180, Springer Nature Limited. Panel **d** reprinted from ref. 175, Springer Nature Limited.

Testing with multiple stressors at once is essential to obtain reliable results. For example, in one study, encapsulated $Cs_{0.05}FA_{0.8}MA_{0.15}Pb(I_{0.85}Br_{0.15})_3$ cells showed no degradation after 2,000 h of IEC standard damp-heat testing. When subjected to MPP tracking under illumination, however, the same cells degraded to 80% of their initial PCE in a few tens of hours under illumination at an elevated temperature (45 °C)[183]. To combat this discrepancy, researchers should compare different ageing conditions individually and in combination. First, researchers should find an encapsulation technique that can allow cells to pass the IEC61215:2016 damp-heat test (85 °C/85% relative humidity), and then operational testing under different light and temperature conditions should be examined. These conditions should include varying light

intensity (0.1 to 10 suns, with and without ultraviolet light), temperature cycling (−40 °C to 85 °C) and light cycling (0 to 1 sun).

Perspective and conclusion

For many years now, stability rather than efficiency has been the most pressing issue in PSC research. In this time, great progress has been made, and the field has produced a toolbox with which we can fabricate highly stable PSCs. Indeed, it should come as no surprise that the strongest operational stability yet reported (ref. 10) used PSCs that are all-inorganic (high-temperature stability), have Cr/Au electrodes, and use 2D perovskite and Al_2O_3 barrier layers. Clearly the field is advancing, and by using many stability-enhancing techniques in parallel, multiyear operational stability has been achieved.

A few final pieces are needed to demonstrate long-term stability: accurate models that allow faster accelerated ageing on a wider range of PSCs, methods to increase predicted T_{80} stability to >25 years and techniques to upscale stable methods for large-area modules. Here, we give our view on how best to approach these challenges.

Modelling degradation

In theory, one can accurately model the degradation from multiple stressors and degradation modes by patiently examining stability curves and fitting them to increasingly complex functions. Instead, it is easier to work on a PSC architecture that is already reasonably robust, which reduces the number of potential degradation modes and simplifies the model. Encapsulating cells in multiple layers and/or using glass–glass lamination seems to negate environmental effects. Then, by using stable transport layers and conformal blocking layers, we can focus on the perovskite film. Limiting temperatures to <90 °C for FA-based perovskites and to <300 °C for inorganic perovskites can restrict unrealistic thermal decomposition. Previous testing suggests that only a few degradation modes are present after such isolation: ion drift, decomposition of PbI to Pb^0 and I^2 gas, cation segregation and halide segregation. Although still a complex system, these processes are governed by ion migration energies and light-induced decomposition, so only a small number of measurements are required. We expect sophisticated models that capture this behaviour to appear soon. Once established, they can be used to accelerate testing protocols further, using high illumination intensities and high temperatures.

Methods to increase perovskite stability

Although impressive increases to PSC stability have been achieved, these results do not yet meet the requirements for commercial application. To further increase stability, additional techniques should be considered in combination with other strategies. We suggest some underappreciated methods below.

Single-crystal PSCs. Single-crystal perovskites are archetypal materials for investigation as they have no grain boundaries and have defect densities several orders of magnitude lower than their polycrystalline counterparts[184–186]. As such, single crystals demonstrate suppressed ion migration, charge accumulation and defect-induced phase transitions[187]. The relatively small number of reports on single-crystal PSCs have shown that single crystals are superior to polycrystalline films at withstanding humidity and heat[188]. Through modified HTL–perovskite interface, $MAPbI_3$ single-crystal devices with 22.1% PCE have been achieved. These devices maintained 90% of their initial PCE after 1,000 h in air, compared with controls maintaining only 61%[189]. Given their inherent advantages, we expect single-crystal PSCs to display impressive stability under operation, but more work is necessary to conclude on the matter.

Quasi-single-crystalline PSCs. We currently lack methods to upscale single-crystal PSCs, and cell areas are limited to ~0.1 cm^2. Quasi-single-crystal film growth (that is, the growth of films composed of micrometre-scale single crystallites through seeded growth) represents a promising middle ground between traditional thin-film processing and single-crystal PSCs. For example, perovskite thin films have been fabricated by first forming a repeating array of 5-µm crystals spaced 5 µm apart, seeding the growth of a continuous film with grain size exceeding 3 µm (ref. 190). Stability tracking of encapsulated devices (FTO/SnO_2/perovskite/PEAI/spiro-OMeTAD/Au, where FTO is fluorine-doped tin oxide) at room temperature under AM1.5 1-sun intensity (ISOS-L1) demonstrated a T_{80} lifetime of 200 h for control devices and a T_{90} of 2,000 h for the seeded growth films (initial PCE ~24%). Optimized PSC architecture could further improve the stability of quasi-single-crystal devices.

Down-conversion layer. Because shorter-wavelength light is the most detrimental to perovskite stability, introducing a barrier layer to absorb ultraviolet light is an obvious way to enhance PSC stability. However, this approach also reduces the short-circuit current density J_{SC} (ref. 56). Using a down-conversion material as a barrier layer solves this issue by absorbing ultraviolet light and converting it into longer (visible) wavelengths. Although this concept has attracted some attention[62], it has mostly been applied to non-optimized $MAPbI_3$ cells in an attempt to increase the current density, rather than to achieve higher stability. Conversion layers with photoluminescent quantum efficiency >80% induce only about a 2% increase in J_{SC}, and this small improvement in current probably does not justify the added cost of the additional layers. These down-conversion layers, however, could be integrated in cells to improve their stability. For example, $MAPbI_3$ cells using a $CsPbCl_3$:Mn quantum dot conversion layer yielded a fourfold increase in stability under ultraviolet light[191]. The use of this method in a highly stable cell architecture is an exciting prospect.

Upscaling stability

Most of the methods described herein were demonstrated on cells with <1 cm^2 active area. Upscaling this to modules involves a change in approach, moving away from spin coating to techniques such as blade coating, slot-die coating, screen printing or vacuum evaporation. These processes have a whole host of new engineering challenges to produce PCEs and stabilities comparable with small-scale, spin-coated devices. For solution-processed films, volatile solvents such as DMSO are usually used, but unevaporated trapped DMSO can escape to produce voids between the perovskite and CTLs. This issue is accentuated in large-area devices causing rapid degradation under light and heat. Using non-volatile carbohydrazide to replace DMSO can overcome this issue. Carbohydrazide is reported to remain in films even after long-term exposure to 1-sun illumination at 60 °C, and 50-cm^2 modules using carbohydrazine have been fabricated[192] with efficiencies approaching 20% PCE and T_{85} lifetimes of 1,000 h under 1-sun illumination at 50 °C. Even more encouraging is the report of a T_{97} > 1 year for 20-cm^2 devices under light cycling, produced by replacing DMSO with another less volatile agent (diphenyl sulfoxide)[193].

In monolithically integrated panels, P2 laser scribing can leave thermally damaged perovskite near the edges of the scribe. Furthermore, if metal is used to fill the via (the trench created in the scribing

process), the direct contact with the perovskite can cause rapid degradation because halides react with metal[194]. Making singulated cells is advantageous to avoid the use of laser scribes. This approach keeps barriers intact, avoids passing metal through the perovskite, avoids thermal damage associated with laser scribing, and allows the binning of cells by efficiency. If singulated cells are connected with a wire, current can be routed around a cell and through a bypass diode to prevent the cell from being pushed into reverse bias if it is in the shade while the other cells are illuminated. Perovskite–silicon tandems naturally take this approach.

These promising results suggest that highly stable modules are achievable. We expect a continued focus on module stability as the field progresses towards commercial stability.

Conclusion

Despite being a persistent problem in perovskite PV, stability has improved by orders of magnitude in the first decade of mainstream perovskite PV research. With the introduction of various stability-enhancing methods, the operational stability of PSCs is maturing beyond practically achievable testing lifetimes. The introduction of degradation modelling and lifetime estimation has suggested that some current PSC configurations could already have lifetimes similar to established PV. Currently, PSC researchers are using the ISOS protocols adapted from OPV research. Further degradation analysis and comparison with outdoor testing is critical to generate perovskite-specific protocols for calculating cell lifetimes and to understand how to improve stability further. Because many factors cause PSC degradation, solving stability issues using only one method is unrealistic, and the synergistic use of various stability-enhancing methods is the way forward. Considering what has already been achieved and the continued huge effort expended in this field, we expect that perovskite solar modules that retain 90% of their initial performance after 25 years of operation will soon emerge.

Published online: 04 August 2023

References

1. Jena, A. K. et al. Halide perovskite photovoltaics: background, status, and future prospects. *Chem. Rev.* **119**, 3036–3103 (2019).
2. Zhu, H. et al. Efficient and stable large bandgap $MAPbBr_3$ perovskite solar cell attaining an open circuit voltage of 1.65 V. *ACS Energy Lett.* **7**, 1112–1119 (2021).
3. Green, M. A. et al. Solar cell efficiency tables (version 60). *Prog. Photovolt. Res. Appl.* **30**, 687–701 (2022).
4. Dualeh, A. et al. Thermal behavior of methylammonium lead-trihalide perovskite photovoltaic light harvesters. *Chem. Mater.* **26**, 6160–6164 (2014).
5. Conings, B. et al. Intrinsic thermal instability of methylammonium lead trihalide perovskite. *Adv. Energy Mater.* **5**, 1500477 (2015).
6. Zhao, X. et al. Room-temperature-processed fullerene single-crystalline nanoparticles for high-performance flexible perovskite photovoltaics. *J. Mater. Chem. A* **7**, 1509–1518 (2019).
7. Kim, G. Y. et al. Large tunable photoeffect on ion conduction in halide perovskites and implications for photodecomposition. *Nat. Mater.* **17**, 445–449 (2018).
8. Leijtens, T. et al. Overcoming ultraviolet light instability of sensitized TiO_2 with meso-superstructured organometal tri-halide perovskite solar cells. *Nat. Commun.* **4**, 2885 (2013).
9. Sidhik, S. et al. Deterministic fabrication of 3D/2D perovskite bilayer stacks for durable and efficient solar cells. *Science* **377**, 1425–1430 (2022).
10. Zhao, X. et al. Accelerated aging of all-inorganic, interface-stabilized perovskite solar cells. *Science* **377**, 307–310 (2022).
11. Grancini, G. et al. One-year stable perovskite solar cells by 2D/3D interface engineering. *Nat. Commun.* **8**, 15684 (2017).
12. Wang, Y. et al. Encapsulation and stability testing of perovskite solar cells for real life applications. *ACS Mater. Au* **2**, 215–236 (2022).
13. Brandt, R. E. et al. Searching for 'defect-tolerant' photovoltaic materials: combined theoretical and experimental screening. *Chem. Mater.* **29**, 4667–4674 (2017).
14. Huang, Y.-T. et al. Perovskite-inspired materials for photovoltaics and beyond — from design to devices. *Nanotechnology* **32**, 132004 (2021).
15. Macpherson, S. et al. Local nanoscale phase impurities are degradation sites in halide perovskites. *Nature* **607**, 294–300 (2022).
16. Fabini, D. H. et al. The underappreciated lone pair in halide perovskites underpins their unusual properties. *MRS Bull.* **45**, 467–477 (2020).
17. Yaffe, O. et al. Local polar fluctuations in lead halide perovskite crystals. *Phys. Rev. Lett.* **118**, 136001 (2017).
18. Bertoluzzi, L. et al. Mobile ion concentration measurement and open-access band diagram simulation platform for halide perovskite solar cells. *Joule* **4**, 109–127 (2020).
19. Eames, C. et al. Ionic transport in hybrid lead iodide perovskite solar cells. *Nat. Commun.* **6**, 7497 (2015).
20. Chen, B. et al. Origin of *J–V* hysteresis in perovskite solar cells. *J. Phys. Chem. Lett.* **7**, 905–917 (2016).
21. Tress, W. et al. Understanding the rate-dependent *J–V* hysteresis, slow time component, and aging in $CH_3NH_3PbI_3$ perovskite solar cells: the role of a compensated electric field. *Energy Environ. Sci.* **8**, 995–1004 (2015).
22. Zhao, Y. et al. A bilayer conducting polymer structure for planar perovskite solar cells with over 1,400 hours operational stability at elevated temperatures. *Nat. Energy* **7**, 144–152 (2022).
23. Yang, T.-Y. et al. The significance of ion conduction in a hybrid organic–inorganic lead-iodide-based perovskite photosensitizer. *Angew. Chem. Int. Ed.* **54**, 7905–7910 (2015).
24. Senocrate, A. et al. Thermochemical stability of hybrid halide perovskites. *ACS Energy Lett.* **4**, 2859–2870 (2019).
25. Boyd, C. C. et al. Understanding degradation mechanisms and improving stability of perovskite photovoltaics. *Chem. Rev.* **119**, 3418–3451 (2018).
26. Lehmann, F. et al. The phase diagram of a mixed halide (Br, I) hybrid perovskite obtained by synchrotron X-ray diffraction. *RSC Adv.* **9**, 11151–11159 (2019).
27. Zhu, T. et al. Coupling photogeneration with thermodynamic modeling of light-induced alloy segregation enables the discovery of stabilizing dopants. Preprint at https://doi.org/10.48550/arXiv.2301.12627 (2023).
28. Brivio, F. et al. Thermodynamic origin of photoinstability in the $CH_3NH_3Pb(I_{1-x}Br_x)_3$ hybrid halide perovskite alloy. *J. Phys. Chem. Lett.* **7**, 1083–1087 (2016).
29. Bischak, C. G. et al. Origin of reversible photoinduced phase separation in hybrid perovskites. *Nano Lett.* **17**, 1028–1033 (2017).
30. Wang, X. et al. Suppressed phase separation of mixed-halide perovskites confined in endotaxial matrices. *Nat. Commun.* **10**, 695 (2019).
31. Belisle, R. A. et al. Impact of surfaces on photoinduced halide segregation in mixed-halide perovskites. *ACS Energy Lett.* **3**, 2694–2700 (2018).
32. Barker, A. J. et al. Defect-assisted photoinduced halide segregation in mixed-halide perovskite thin films. *ACS Energy Lett.* **2**, 1416–1424 (2017).
33. Kerner, R. A. et al. The role of halide oxidation in perovskite halide phase separation. *Joule* **5**, 2273–2295 (2021).
34. DuBose, J. T. & Kamat, P. V. Hole trapping in halide perovskites induces phase segregation. *Acc. Mater. Res.* **3**, 761–771 (2022).
35. Khenkin, M. V. et al. Consensus statement for stability assessment and reporting for perovskite photovoltaics based on ISOS procedures. *Nat. Energy* **5**, 35–49 (2020).
36. Burschka, J. et al. Sequential deposition as a route to high-performance perovskite-sensitized solar cells. *Nature* **499**, 316–320 (2013).
37. Jiang, Q. et al. Surface passivation of perovskite film for efficient solar cells. *Nat. Photonics* **13**, 460–466 (2019).
38. Min, H. et al. Efficient, stable solar cells by using inherent bandgap of α-phase formamidinium lead iodide. *Science* **366**, 749–753 (2019).
39. Zhao, Y. et al. Inactive $(PbI_2)_2RbCl$ stabilizes perovskite films for efficient solar cells. *Science* **377**, 531–534 (2022).
40. Saliba, M. et al. Incorporation of rubidium cations into perovskite solar cells improves photovoltaic performance. *Science* **354**, 206–209 (2016).
41. Jost, M. et al. Perovskite solar cells go outdoors: field testing and temperature effects on energy yield. *Adv. Energy Mater.* **10**, 2000454 (2020).
42. Emery, Q. et al. Encapsulation and outdoor testing of perovskite solar cells: comparing industrially relevant process with a simplified lab procedure. *ACS Appl. Mater. Interfaces* **14**, 5159–5167 (2022).
43. Pescetelli, S. et al. Integration of two-dimensional materials-based perovskite solar panels into a stand-alone solar farm. *Nat. Energy* **7**, 597–607 (2022).
44. Li, Z. et al. Stabilizing perovskite structures by tuning tolerance factor: formation of formamidinium and cesium lead iodide solid-state alloys. *Chem. Mater.* **28**, 284–292 (2016).
45. Stoumpos, C. C. et al. Semiconducting tin and lead iodide perovskites with organic cations: phase transitions, high mobilities, and near-infrared photoluminescent properties. *Inorg. Chem.* **52**, 9019–9038 (2013).
46. Fabini, D. H. et al. Reentrant structural and optical properties and large positive thermal expansion in perovskite formamidinium lead iodide. *Angew. Chem. Int. Ed.* **55**, 15392–15396 (2016).
47. Cao, D. H. et al. 2D homologous perovskites as light-absorbing materials for solar cell applications. *J. Am. Chem. Soc.* **137**, 7843–7850 (2015).
48. Choi, K. et al. Heat dissipation effects on the stability of planar perovskite solar cells. *Energy Environ. Sci.* **13**, 5059–5067 (2020).
49. Brunetti, B. et al. On the thermal and thermodynamic (in)stability of methylammonium lead halide perovskites. *Sci. Rep.* **6**, 31896 (2016).

50. Eperon, G. E. et al. Formamidinium lead trihalide: a broadly tunable perovskite for efficient planar heterojunction solar cells. *Energy Environ. Sci.* **7**, 982–988 (2014).
51. Liu, Z. et al. Efficient and stable FA-rich perovskite photovoltaics: from material properties to device optimization. *Adv. Energy Mater.* **12**, 2200111 (2022).
52. Juarez-Perez, E. J. et al. Thermal degradation of formamidinium based lead halide perovskites into *sym*-triazine and hydrogen cyanide observed by coupled thermogravimetry–mass spectrometry analysis. *J. Mater. Chem. A* **7**, 16912–16919 (2019).
53. Pang, S. et al. $NH_2CH{=}NH_2PbI_3$: an alternative organolead iodide perovskite sensitizer for mesoscopic solar cells. *Chem. Mater.* **26**, 1485–1491 (2014).
54. Burwig, T. et al. Crystal phases and thermal stability of co-evaporated $CsPbX_3$ (X=I, Br) thin films. *J. Phys. Chem. Lett.* **9**, 4808–4813 (2018).
55. Lee, S.-W. et al. UV degradation and recovery of perovskite solar cells. *Sci. Rep.* **6**, 38150 (2016).
56. Wang, Z. et al. Recent advances and perspectives of photostability for halide perovskite solar cells. *Adv. Opt. Mater.* **10**, 2101822 (2022).
57. Lang, F. et al. Influence of radiation on the properties and the stability of hybrid perovskites. *Adv. Mater.* **30**, 1702905 (2018).
58. Juarez-Perez, E. J. et al. Photodecomposition and thermal decomposition in methylammonium halide lead perovskites and inferred design principles to increase photovoltaic device stability. *J. Mater. Chem. A* **6**, 9604–9612 (2018).
59. Dawood, R. I. et al. The photodecomposition of lead iodide. *Proc. R. Soc. Lond. A* **284**, 272–288 (1965).
60. Nickel, N. H. et al. Unraveling the light-induced degradation mechanisms of $CH_3NH_3PbI_3$ perovskite films. *Adv. Electron. Mater.* **3**, 1700158 (2017).
61. Donakowski, A. et al. Improving photostability of cesium-doped formamidinium lead triiodide perovskite. *ACS Energy Lett.* **6**, 574–580 (2021).
62. Hoke, E. T. et al. Reversible photo-induced trap formation in mixed-halide hybrid perovskites for photovoltaics. *Chem. Sci.* **6**, 613–617 (2015).
63. Mahesh, S. et al. Revealing the origin of voltage loss in mixed-halide perovskite solar cells. *Energy Environ. Sci.* **13**, 258–267 (2020).
64. Bai, Y. et al. Initializing film homogeneity to retard phase segregation for stable perovskite solar cells. *Science* **378**, 747–754 (2022).
65. Lan, D. et al. Combatting temperature and reverse-bias challenges facing perovskite solar cells. *Joule* **6**, 1782–1797 (2022).
66. Bowring, A. R. et al. Reverse bias behavior of halide perovskite solar cells. *Adv. Energy Mater.* **8**, 1702365 (2018).
67. Bertoluzzi, L. et al. Incorporating electrochemical halide oxidation into drift-diffusion models to explain performance losses in perovskite solar cells under prolonged reverse bias. *Adv. Energy Mater.* **11**, 2002614 (2021).
68. Razera, R. A. Z. et al. Instability of p-i-n perovskite solar cells under reverse bias. *J. Mater. Chem. A* **8**, 242–250 (2020).
69. Wolf, E. J. et al. Designing modules to prevent reverse bias degradation in perovskite solar cells when partial shading occurs. *Sol. RRL* **6**, 2100239 (2022).
70. Ni, Z. et al. Resolving spatial and energetic distributions of trap states in metal halide perovskite solar cells. *Science* **367**, 1352–1358 (2020).
71. Wang, J. et al. Photoinduced dynamic defects responsible for the giant, reversible, and bidirectional light-soaking effect in perovskite solar cells. *J. Phys. Chem. Lett.* **12**, 9328–9335 (2021).
72. Xu, B. et al. Bifunctional spiro-fluorene/heterocycle cored hole-transporting materials: role of the heteroatom on the photovoltaic performance of perovskite solar cells. *Chem. Eng. J.* **431**, 133371 (2022).
73. Luo, D. et al. Minimizing non-radiative recombination losses in perovskite solar cells. *Nat. Rev. Mater.* **5**, 44–60 (2019).
74. Reichert, S. et al. Probing the ionic defect landscape in halide perovskite solar cells. *Nat. Commun.* **11**, 6098 (2020).
75. Xue, J. et al. The surface of halide perovskites from nano to bulk. *Nat. Rev. Mater.* **5**, 809–827 (2020).
76. Azpiroz, J. M. et al. Defect migration in methylammonium lead iodide and its role in perovskite solar cell operation. *Energy Environ. Sci.* **8**, 2118–2127 (2015).
77. Chen, C. et al. Arylammonium-assisted reduction of the open-circuit voltage deficit in wide-bandgap perovskite solar cells: the role of suppressed ion migration. *ACS Energy Lett.* **5**, 2560–2568 (2020).
78. Liu, J. et al. Correlations between electrochemical ion migration and anomalous device behaviors in perovskite solar cells. *ACS Energy Lett.* **6**, 1003–1014 (2021).
79. McGovern, L. et al. Reduced barrier for ion migration in mixed-halide perovskites. *ACS Appl. Energy Mater.* **4**, 13431–13437 (2021).
80. Yang, S. et al. Stabilizing halide perovskite surfaces for solar cell operation with wide-bandgap lead oxysalts. *Science* **365**, 473–478 (2019).
81. Ahn, N. et al. Trapped charge-driven degradation of perovskite solar cells. *Nat. Commun.* **7**, 13422 (2016).
82. Wang, Q. et al. Scaling behavior of moisture-induced grain degradation in polycrystalline hybrid perovskite thin films. *Energy Environ. Sci.* **10**, 516–522 (2017).
83. Samu, G. F. et al. Electrochemical hole injection selectively expels iodide from mixed halide perovskite films. *J. Am. Chem. Soc.* **141**, 10812–10820 (2019).
84. Ni, Z. et al. Evolution of defects during the degradation of metal halide perovskite solar cells under reverse bias and illumination. *Nat. Energy* **7**, 65–73 (2022).
85. Lin, C.-H. et al. Electrode engineering in halide perovskite electronics: plenty of room at the interfaces. *Adv. Mater.* **34**, 2108616 (2022).
86. Back, H. et al. Achieving long-term stable perovskite solar cells via ion neutralization. *Energy Environ. Sci.* **9**, 1258–1263 (2016).
87. Domanski, K. et al. Not all that glitters is gold: metal-migration-induced degradation in perovskite solar cells. *ACS Nano* **10**, 6306–6314 (2016).
88. Guerrero, A. et al. Interfacial degradation of planar lead halide perovskite solar cells. *ACS Nano* **10**, 218–224 (2016).
89. Zhen, C. et al. Strategies for modifying TiO_2 based electron transport layers to boost perovskite solar cells. *ACS Sustain. Chem. Eng.* **7**, 4586–4618 (2019).
90. Sakhatskyi, K. et al. Assessing the drawbacks and benefits of ion migration in lead halide perovskites. *ACS Energy Lett.* **7**, 3401–3414 (2022).
91. Ito, S. et al. Effects of surface blocking layer of Sb_2S_3 on nanocrystalline TiO_2 for $CH_3NH_3PbI_3$ perovskite solar cells. *J. Phys. Chem. C.* **118**, 16995–17000 (2014).
92. Boldyreva, A. G. et al. Unraveling the impact of hole transport materials on photostability of perovskite films and p-i-n solar cells. *ACS Appl. Mater. Interfaces* **12**, 19161–19173 (2020).
93. Zhu, H. et al. Low-cost dopant additive-free hole-transporting material for a robust perovskite solar cell with efficiency exceeding 21%. *ACS Energy Lett.* **6**, 208–215 (2021).
94. Bauer, M. et al. Cyclopentadiene-based hole-transport material for cost-reduced stabilized perovskite solar cells with power conversion efficiencies over 23%. *Adv. Energy Mater.* **11**, 2003953 (2021).
95. Fu, Q. et al. Ionic dopant-free polymer alloy hole transport materials for high-performance perovskite solar cells. *J. Am. Chem. Soc.* **144**, 9500–9509 (2022).
96. Habisreutinger, S. N. et al. Dopant-free planar n-i-p perovskite solar cells with steady-state efficiencies exceeding 18%. *ACS Energy Lett.* **2**, 622–628 (2017).
97. Li, W. et al. Montmorillonite as bifunctional buffer layer material for hybrid perovskite solar cells with protection from corrosion and retarding recombination. *J. Mater. Chem. A* **2**, 13587–13592 (2014).
98. Tao, S. et al. Absolute energy level positions in tin- and lead-based halide perovskites. *Nat. Commun.* **10**, 2560 (2019).
99. Prasanna, R. et al. Band gap tuning via lattice contraction and octahedral tilting in perovskite materials for photovoltaics. *J. Am. Chem. Soc.* **139**, 11117–11124 (2017).
100. Chen, H. et al. Advances to high-performance black-phase $FAPbI_3$ perovskite for efficient and stable photovoltaics. *Small Struct.* **2**, 2000130 (2021).
101. Pellet, N. et al. Mixed-organic-cation perovskite photovoltaics for enhanced solar-light harvesting. *Angew. Chem. Int. Ed.* **53**, 3151–3157 (2014).
102. Lee, J.-W. et al. Formamidinium and cesium hybridization for photo- and moisture-stable perovskite solar cell. *Adv. Energy Mater.* **5**, 1501310 (2015).
103. Zhao, Y. et al. Discovery of temperature-induced stability reversal in perovskites using high-throughput robotic learning. *Nat. Commun.* **12**, 2191 (2021).
104. Saliba, M. et al. Cesium-containing triple cation perovskite solar cells: improved stability, reproducibility and high efficiency. *Energy Environ. Sci.* **9**, 1989–1997 (2016).
105. Jeong, J. et al. Pseudo-halide anion engineering for α-$FAPbI_3$ perovskite solar cells. *Nature* **592**, 381–385 (2021).
106. Yun, H.-S. et al. Ethanol-based green-solution processing of α-formamidinium lead triiodide perovskite layers. *Nat. Energy* **7**, 828–834 (2022).
107. Doherty, T. A. S. et al. Stabilized tilted-octahedra halide perovskites inhibit local formation of performance-limiting phases. *Science* **374**, 1598–1605 (2021).
108. Mundt, L. E. et al. Mixing matters: nanoscale heterogeneity and stability in metal halide perovskite solar cells. *ACS Energy Lett.* **7**, 471–480 (2021).
109. Grancini, G. et al. Dimensional tailoring of hybrid perovskites for photovoltaics. *Nat. Rev. Mater.* **4**, 4–22 (2019).
110. Shi, E. et al. Two-dimensional halide perovskite nanomaterials and heterostructures. *Chem. Soc. Rev.* **47**, 6046–6072 (2018).
111. Quan, L. N. et al. Ligand-stabilized reduced-dimensionality perovskites. *J. Am. Chem. Soc.* **138**, 2649–2655 (2016).
112. An, Y. et al. Structural stability of formamidinium- and cesium-based halide perovskites. *ACS Energy Lett.* **6**, 1942–1969 (2021).
113. Beal, R. E. et al. Cesium lead halide perovskites with improved stability for tandem solar cells. *J. Phys. Chem. Lett.* **7**, 746–751 (2016).
114. Liu, Y. et al. Stabilization of highly efficient and stable phase-pure $FAPbI_3$ perovskite solar cells by molecularly tailored 2D-overlayers. *Angew. Chem. Int. Ed.* **59**, 15688 (2020).
115. Fan, Y. et al. The chemical design in high-performance lead halide perovskite: additive vs dopant? *J. Phys. Chem. Lett.* **12**, 11636–11644 (2021).
116. Ling, X. et al. Combined precursor engineering and grain anchoring leading to MA-free, phase-pure, and stable α-formamidinium lead iodide perovskites for efficient solar cells. *Angew. Chem. Int. Ed.* **60**, 27299–27306 (2021).
117. Kim, M. et al. Methylammonium chloride induces intermediate phase stabilization for efficient perovskite solar cells. *Joule* **3**, 2179–2192 (2019).
118. Xu, J. et al. Triple-halide wide band gap perovskites with suppressed phase segregation for efficient tandems. *Science* **367**, 1097–1104 (2020).
119. Chen, R. et al. Moisture-tolerant and high-quality α-$CsPbI_3$ films for efficient and stable perovskite solar modules. *J. Mater. Chem. A* **8**, 9597–9606 (2020).
120. Li, T. et al. Inorganic wide-bandgap perovskite subcells with dipole bridge for all-perovskite tandems. *Nat. Energy* **8**, 610–620 (2023).
121. Wang, Y. et al. Thermodynamically stabilized β-$CsPbI_3$-based perovskite solar cells with efficiencies >18%. *Science* **365**, 591–595 (2019).
122. Chu, X. et al. Surface in situ reconstruction of inorganic perovskite films enabling long carrier lifetimes and solar cells with 21% efficiency. *Nat. Energy* **8**, 372–380 (2023).

123. Park, J. et al. Controlled growth of perovskite layers with volatile alkylammonium chlorides. *Nature* **616**, 724–730 (2023).
124. Zhang, S. et al. Barrier designs in perovskite solar cells for long-term stability. *Adv. Energy Mater.* **10**, 2001610 (2020).
125. Hou, F. et al. Efficient and stable planar heterojunction perovskite solar cells with an MoO_3/PEDOT:PSS hole transporting layer. *Nanoscale* **7**, 9427–9432 (2015).
126. Kim, J. M. et al. Use of $AuCl_3$-doped graphene as a protecting layer for enhancing the stabilities of inverted perovskite solar cells. *Appl. Surf. Sci.* **455**, 1131–1136 (2018).
127. Akin Kara, D. et al. Enhanced device efficiency and long-term stability via boronic acid-based self-assembled monolayer modification of ITO in planar perovskite solar cell. *ACS Appl. Mater. Interfaces* **10**, 30000–30007 (2018).
128. Wu, S. et al. A chemically inert bismuth interlayer enhances long-term stability of inverted perovskite solar cells. *Nat. Commun.* **10**, 1161 (2019).
129. Chen, H. et al. Regulating surface potential maximizes voltage in all-perovskite tandems. *Nature* **613**, 676–681 (2022).
130. Bush, K. A. et al. 23.6%-efficient monolithic perovskite/silicon tandem solar cells with improved stability. *Nat. Energy* **2**, 17009 (2017).
131. Wu, Z. et al. Highly efficient and stable perovskite solar cells via modification of energy levels at the perovskite/carbon electrode interface. *Adv. Mater.* **31**, 1804284 (2019).
132. McGott, D. L. et al. 3D/2D passivation as a secret to success for polycrystalline thin-film solar cells. *Joule* **5**, 1057–1073 (2021).
133. Lintangpradipto, M. N. et al. Size-controlled CdSe quantum dots to boost light harvesting capability and stability of perovskite photovoltaic cells. *Nanoscale* **9**, 10075–10083 (2017).
134. Kot, M. et al. Room temperature atomic layer deposited Al_2O_3 improves perovskite solar cells efficiency over time. *ChemSusChem* **11**, 3640–3648 (2018).
135. Palmstrom, A. F. et al. Interfacial effects of tin oxide atomic layer deposition in metal halide perovskite photovoltaics. *Adv. Energy Mater.* **8**, 1800591 (2018).
136. Tan, F. et al. In situ back-contact passivation improves photovoltage and fill factor in perovskite solar cells. *Adv. Mater.* **31**, 1807435 (2019).
137. He, Q. et al. Highly efficient and stable perovskite solar cells enabled by low-cost industrial organic pigment coating. *Angew. Chem. Int. Ed.* **60**, 2485–2492 (2021).
138. Wu, Y. et al. Interface modification to achieve high-efficiency and stable perovskite solar cells. *Chem. Eng. J.* **433**, 134613 (2022).
139. Wu, Y. et al. Realizing high-efficiency perovskite solar cells by passivating triple-cation perovskite films. *Sol. RRL* **6**, 2200115 (2022).
140. Zhu, H. et al. Tailored amphiphilic molecular mitigators for stable perovskite solar cells with 23.5% efficiency. *Adv. Mater.* **32**, 1907757 (2020).
141. Chen, H. et al. Quantum-size-tuned heterostructures enable efficient and stable inverted perovskite solar cells. *Nat. Photonics* **16**, 352–358 (2022).
142. Azmi, R. et al. Damp heat-stable perovskite solar cells with tailored-dimensionality 2D/3D heterojunctions. *Science* **376**, 73–77 (2022).
143. Jang, Y.-W. et al. Intact 2D/3D halide junction perovskite solar cells via solid-phase in-plane growth. *Nat. Energy* **6**, 63–71 (2021).
144. Li, Z. et al. Organometallic-functionalized interfaces for highly efficient inverted perovskite solar cells. *Science* **376**, 416–420 (2022).
145. Saidaminov, M. I. et al. Suppression of atomic vacancies via incorporation of isovalent small ions to increase the stability of halide perovskite solar cells in ambient air. *Nat. Energy* **3**, 648–654 (2018).
146. Zhu, H. et al. Suppressing defects through thiadiazole derivatives that modulate $CH_3NH_3PbI_3$ crystal growth for highly stable perovskite solar cells under dark conditions. *J. Mater. Chem. A* **6**, 4971–4980 (2018).
147. Zhou, T. et al. Crystal growth regulation of 2D/3D perovskite films for solar cells with both high efficiency and stability. *Adv. Mater.* **34**, 2200705 (2022).
148. Yu, S. et al. Hydrazinium cation mixed $FAPbI_3$-based perovskite with 1D/3D hybrid dimension structure for efficient and stable solar cells. *Chem. Eng. J.* **403**, 125724 (2020).
149. Rahman, S. I. et al. Grain boundary defect passivation of triple cation mixed halide perovskite with hydrazine-based aromatic iodide for efficiency improvement. *ACS Appl. Mater. Interfaces* **12**, 41312–41322 (2020).
150. Luo, J. et al. Application of ionic liquids and derived materials to high-efficiency and stable perovskite solar cells. *ACS Mater. Lett.* **4**, 1684–1715 (2022).
151. Lee, J.-W. et al. Lewis acid–base adduct approach for high efficiency perovskite solar cells. *Acc. Chem. Res.* **49**, 311–319 (2016).
152. Han, T.-H. et al. Perovskite–polymer composite cross-linker approach for highly-stable and efficient perovskite solar cells. *Nat. Commun.* **10**, 520 (2019).
153. Lao, Y. et al. Multifunctional π-conjugated additives for halide perovskite. *Adv. Sci.* **9**, 2105307 (2022).
154. Lin, Y. et al. π-Conjugated Lewis base: efficient trap-passivation and charge-extraction for hybrid perovskite solar cells. *Adv. Mater.* **29**, 1604545 (2017).
155. Bi, D. et al. Polymer-templated nucleation and crystal growth of perovskite films for solar cells with efficiency greater than 21%. *Nat. Energy* **1**, 16142 (2016).
156. Wang, R. et al. Constructive molecular configurations for surface-defect passivation of perovskite photovoltaics. *Science* **366**, 1509–1513 (2019).
157. Li, C. et al. Rational design of Lewis base molecules for stable and efficient inverted perovskite solar cells. *Science* **379**, 690–694 (2023).
158. Zheng, X. et al. Managing grains and interfaces via ligand anchoring enables 22.3%-efficiency inverted perovskite solar cells. *Nat. Energy* **5**, 131–140 (2020).
159. Kim, M. et al. Conformal quantum dot-SnO_2 layers as electron transporters for efficient perovskite solar cells. *Science* **375**, 302–306 (2022).
160. Zhang, F. et al. The impact of peripheral groups on phenothiazine-based hole-transporting materials for perovskite solar cells. *ACS Energy Lett.* **3**, 1145–1152 (2018).
161. Zhang, F. et al. Over 20% PCE perovskite solar cells with superior stability achieved by novel and low-cost hole-transporting materials. *Nano Energy* **41**, 469–475 (2017).
162. Dong, Y. et al. Simple 9,10-dihydrophenanthrene based hole-transporting materials for efficient perovskite solar cells. *Chem. Eng. J.* **402**, 126298 (2020).
163. Zhang, J. et al. 4-*tert*-Butylpyridine free hole transport materials for efficient perovskite solar cells: a new strategy to enhance the environmental and thermal stability. *ACS Energy Lett.* **3**, 1677–1682 (2018).
164. Shen, Y. et al. crowning lithium ions in hole transport layer toward stable perovskite solar cells. *Adv. Mater.* **34**, 2200978 (2022).
165. Han, Y. et al. Azide additive acting as a powerful locker for Li+ and TBP in spiro-OMeTAD toward highly efficient and stable perovskite solar cells. *Nano Energy* **96**, 107072 (2022).
166. Zhu, H. et al. Synergistic effect of fluorinated passivator and hole transport dopant enables stable perovskite solar cells with an efficiency near 24%. *J. Am. Chem. Soc.* **143**, 3231–3237 (2021).
167. Chen, C. et al. Cu(II) complexes as p-type dopants in efficient perovskite solar cells. *ACS Energy Lett.* **2**, 497–503 (2017).
168. Zhang, T. et al. Ion-modulated radical doping of spiro-OMeTAD for more efficient and stable perovskite solar cells. *Science* **377**, 495–501 (2022).
169. Zhu, H. et al. Dopant-free hole-transport material with a tetraphenylethene core for efficient perovskite solar cells. *Energy Technol.* **5**, 1257–1264 (2017).
170. Cao, J. et al. Ultrathin self-assembly two-dimensional metal-organic framework films as hole transport layers in ideal-bandgap perovskite solar cells. *ACS Energy Lett.* **7**, 3362–3369 (2022).
171. Zhang, H. et al. Low-temperature solution-processed $CuCrO_2$ hole-transporting layer for efficient and photostable perovskite solar cells. *Adv. Energy Mater.* **8**, 1702762 (2018).
172. Arora, N. et al. Perovskite solar cells with CuSCN hole extraction layers yield stabilized efficiencies greater than 20%. *Science* **358**, 768–771 (2017).
173. Fu, Q. et al. Management of donor and acceptor building blocks in dopant-free polymer hole transport materials for high-performance perovskite solar cells. *Angew. Chem. Int. Ed. Engl.* **134**, e202210356 (2022).
174. Rosenthal, A. L. A. D. et al. A ten year review of performance of photovoltaic systems. in *Conference Record of the IEEE Photovoltaic Specialists Conference* 1289–1291 (IEEE, 1993).
175. Domanski, K. et al. Systematic investigation of the impact of operation conditions on the degradation behaviour of perovskite solar cells. *Nat. Energy* **3**, 61–67 (2018).
176. Saliba, M. et al. Measuring aging stability of perovskite solar cells. *Joule* **2**, 1019–1024 (2018).
177. Wu, S. et al. 2D metal–organic framework for stable perovskite solar cells with minimized lead leakage. *Nat. Nanotechnol.* **15**, 934–940 (2020).
178. Haillant, O., Dumbleton, D. & Zielnik, A. An Arrhenius approach to estimating organic photovoltaic module weathering acceleration factors. *Sol. Energy Mater. Sol. Cell* **95**, 1889–1895 (2011).
179. Siegler, T. D. et al. Water-accelerated photooxidation of $CH_3NH_3PbI_3$ perovskite. *J. Am. Chem. Soc.* **144**, 5552–5561 (2022).
180. Wang, Z. et al. High irradiance performance of metal halide perovskites for concentrator photovoltaics. *Nat. Energy* **3**, 855–861 (2018).
181. Tress, W. et al. Performance of perovskite solar cells under simulated temperature-illumination real-world operating conditions. *Nat. Energy* **4**, 568–574 (2019).
182. Anoop, K. M. et al. Bias-dependent stability of perovskite solar cells studied using natural and concentrated sunlight. *Sol. RRL* **4**, 1900335 (2020).
183. Shi, L. et al. Gas chromatography-mass spectrometry analyses of encapsulated stable perovskite solar cells. *Science* **368**, eaba2412 (2020).
184. Shi, D. et al. Low trap-state density and long carrier diffusion in organolead trihalide perovskite single crystals. *Science* **347**, 519–522 (2015).
185. Brenner, T. M. et al. Hybrid organic–inorganic perovskites: low-cost semiconductors with intriguing charge-transport properties. *Nat. Rev. Mater.* **1**, 15007 (2016).
186. Turedi, B. et al. Single-crystal perovskite solar cells exhibit close to half a millimeter electron diffusion length. *Adv. Mater.* **34**, 2202390 (2022).
187. Lee, K. J. et al. Domain-size-dependent residual stress governs the phase-transition and photoluminescence behavior of methylammonium lead iodide. *Adv. Funct. Mater.* **31**, 2008088 (2021).
188. Murali, B. et al. Single crystals: the next big wave of perovskite optoelectronics. *ACS Mater. Lett.* **2**, 184–214 (2020).
189. Li, N. et al. Engineering the hole extraction interface enables single-crystal $MAPbI_3$ perovskite solar cells with efficiency exceeding 22% and superior indoor response. *Adv. Energy Mater.* **12**, 2103241 (2022).
190. Shen, Z. et al. Crystal-array-assisted growth of a perovskite absorption layer for efficient and stable solar cells. *Energy Environ. Sci.* **15**, 1078–1085 (2022).
191. Wang, Q. et al. Energy-down-shift $CsPbCl_3$:Mn quantum dots for boosting the efficiency and stability of perovskite solar cells. *ACS Energy Lett.* **2**, 1479–1486 (2017).
192. Chen, S. et al. Stabilizing perovskite–substrate interfaces for high-performance perovskite modules. *Science* **373**, 902–907 (2021).
193. Yang, Z. et al. Slot-die coating large-area formamidinium-cesium perovskite film for efficient and stable parallel solar module. *Sci. Adv.* **7**, eabg3749 (2021).
194. Zhang, D. et al. Degradation pathways in perovskite solar cells and how to meet international standards. *Commun. Mater.* **3**, 58 (2022).

195. Maier, J. Light gets ions going. *Max Planck Institute for Solid State Research* https://www.fkf.mpg.de/7824789/news_publication_12009261_transferred (18 April 2018).
196. Huang, Z. et al. Suppressed ion migration in reduced-dimensional perovskites improves operating stability. *ACS Energy Lett.* **4**, 1521–1527 (2019).
197. Knight, A. J. et al. Halide segregation in mixed-halide perovskites: influence of A-site cations. *ACS Energy Lett.* **6**, 799–808 (2021).
198. Jacobsson, T. J. et al. An open-access database and analysis tool for perovskite solar cells based on the FAIR data principles. *Nat. Energy* **7**, 107–115 (2022).
199. Jiang, Q. et al. Surface reaction for efficient and stable inverted perovskite solar cells. *Nature* **611**, 278–283 (2022).
200. Pitaro, M. et al. Tin halide perovskites: from fundamental properties to solar cells. *Adv. Mater.* **34**, e2105844 (2021).
201. Tao, L. et al. Stability of mixed-halide wide bandgap perovskite solar cells: strategies and progress. *J. Energy Chem.* **61**, 395–415 (2021).

Acknowledgements
H.Z., S.T., M.N.L., S.M., B.C., E.H.S. and O.M.B. acknowledge funding support from Saudi Aramco. S.T. was supported by the Hatch Graduate scholarship.

Author contributions
H.Z. and S.T. contributed equally to the article. H.Z., S.T., M.N.L., S.M. and B.C. researched data for the article. All authors contributed substantially to discussion of the content. All authors wrote the article. O.M.B., H.Z., S.T., M.D.M. and E.H.S. reviewed and/or edited the manuscript before submission.

Competing interests
M.D.M. is an adviser to Swift Solar. The other authors declare no competing interests.

Additional information
Supplementary information The online version contains supplementary material available at https://doi.org/10.1038/s41578-023-00582-w.

Peer review information *Nature Reviews Materials* thanks Michael Saliba and the other, anonymous, reviewer(s) for their contribution to the peer review of this work.